Received: 29 May 2021 | Revised: 22 June 2021 | Accepted: 2 July 2021

DOI: 10.1002/cne.25213

RESEARCH ARTICLE

JCN RESEARCH IN SYSTEMS NEUROSCIENCE THE JOURNAL OF COMPARATIVE NEUROLOGY WILEY

Ephrin-A3 is required for tonotopic map precision and auditory functions in the mouse auditory brainstem

Natalia Hoshino[1] | Yazan Altarshan[1] | Ahmad Alzein[1] | Amali M. Fernando[1] | Hieu T. Nguyen[1] | Emma F. Majewski[1] | Vincent C.-F. Chen[2] | M. William Rochlin[1] | Wei-Ming Yu[1]

[1]Department of Biology, Loyola University of Chicago, Chicago, Illinois

[2]Engineering Program, Loyola University of Chicago, Chicago, Illinois

Correspondence
Wei-Ming Yu, Department of Biology, Loyola University of Chicago, 1032 W Sheridan Rd, LSB 243, Chicago, IL 60660, USA.
Email: wyu1@luc.edu

Funding information
National Institute on Deafness and Other Communication Disorders, Grant/Award Numbers: R15DC016407, R15DC017866

Abstract

Tonotopy is a prominent feature of the vertebrate auditory system and forms the basis for sound discrimination, but the molecular mechanism that underlies its formation remains largely elusive. Ephrin/Eph signaling is known to play important roles in axon guidance during topographic mapping in other sensory systems, so we investigated its possible role in the establishment of tonotopy in the mouse cochlear nucleus. We found that ephrin-A3 molecules are differentially expressed along the tonotopic axis in the cochlear nucleus during innervation. Ephrin-A3 forward signaling is sufficient to repel auditory nerve fibers in a developmental stage-dependent manner. In mice lacking ephrin-A3, the tonotopic map is degraded and isofrequency bands of neuronal activation upon pure tone exposure become imprecise in the anteroventral cochlear nucleus. Ephrin-A3 mutant mice also exhibit a delayed second wave in auditory brainstem responses upon sound stimuli and impaired detection of sound frequency changes. Our findings establish an essential role for ephrin-A3 in forming precise tonotopy in the auditory brainstem to ensure accurate sound discrimination.

KEYWORDS
auditory nerve fiber, cochlear nucleus, ephrin-A3, frequency discrimination, RRID: AB_2156476, RRID: AB_2314836, RRID: AB_2532109, RRID: AB_2564645, RRID: AB_2744644, RRID: AB_531793, RRID: AB_887864, RRID: AB_94881, spiral ganglion neurons, tonotopy

1 | INTRODUCTION

Tonotopy is a fundamental organizing principle of the vertebrate auditory system (Kandler et al., 2009). Tonotopy originates from the orderly coding of high- to low-frequency sounds by hair cells and their afferents, spiral ganglion neurons (SGNs), along the base to apex of the cochlea. SGNs responding to high-frequency sounds at the cochlear base extend auditory nerve fibers (ANFs) to the dorsal portions of the dorsal cochlear nucleus (DCN), the posteroventral cochlear nucleus, and the anteroventral cochlear nucleus (AVCN). SGNs responding to low-frequency sounds send fibers to the ventral parts of the three cochlear nucleus (CN) subdivisions (Fekete et al., 1984). Thus, ANFs with similar frequency preference terminate within well-defined isofrequency bands in the CN (Muniak et al., 2013).

During development, SGNs are born in a basal-to-apical progression along the cochlea from mouse embryonic day (E) 9.5–10.5 to around E12.5–13.5 (Koundakjian et al., 2007; Matei et al., 2005; Ruben, 1967; Shepard et al., 2019), resulting in ANFs innervating the CN in a developmental gradient according to tonotopy (Scheffel et al., 2020). ANFs from early-born basal SGNs initiate outgrowth and invade the CN by E13.5, about 2–3 days earlier than ANFs from the late-born apical SGNs. In mice, neurogenesis in the CN mainly occurs between E10.5 to E13.5 but some DCN neurons are continuously produced until early postnatal stages (Martin & Rickets, 1981;

Pierce, 1967; Shepard et al., 2019). Despite the ongoing neurogenesis, ANF innervation in the CN is already organized into a coarse tonotopic map by E15.5 (Koundakjian et al., 2007; Scheffel et al., 2020), suggesting that tonotopic map emergence in the CN is primarily specified by molecular cues. Despite its importance, the molecular mechanisms that underlie tonotopic map formation in central auditory circuits remain largely elusive.

A degraded tonotopic map in the auditory brainstem has been observed in mice carrying mutations in several molecules (Clause et al., 2014; Karmakar et al., 2017; Lu et al., 2014; Macova et al., 2019; Yang et al., 2017), but this is thought to result from other developmental defects. To begin our investigation of axon guidance mechanisms that could be important in tonotopy, we focused on ephrins and Ephs, a group of cell–cell recognition molecules that play essential roles in axon pathfinding and targeting (Cramer & Miko, 2016; Kania & Klein, 2016). Ephrins are divided into GPI-linked ephrin-As and transmembrane ephrin-Bs. Five mammalian ephrin-As (ephrin-A1-5, encoded by *Efna1-5*) and three mammalian ephrin-Bs (ephrin-B1-3, encoded by *EfnB1-3*) have been identified. Ephrins interact with 16 known Eph receptors, which are divided into EphA and EphB subclasses. EphAs (EphA1-10) primarily bind to ephrin-As and EphBs (EphB1-6) mainly interact with ephrin-Bs. Although Ephs and ephrins are referred to as receptors and ligands, respectively, both can initiate signaling cascades: forward signaling when Ephs are the receptors, and reverse signaling when Ephs are the ligands. As ephrins and Ephs are expressed on the cell surface, activation of ephrin-Eph signaling is cell contact dependent, allowing highly specific spatial instruction (Egea & Klein, 2007). Ephrin-Eph signaling was first implicated in tonotopic mapping by the pioneering studies of Cramer et al. (Cramer & Gabriele, 2014; Huffman & Cramer, 2007; Miko et al., 2007; Miko et al., 2008; Siddiqui & Cramer, 2005). In chicken embryos, multiple ephrins and Ephs show graded expression in the cochlea and auditory brainstem. In EphA4- and ephrin-B2-deficient mice, they respond to sounds with decreased sensitivity and increased latency and exhibit altered auditory activation patterns in auditory brainstem nuclei. These findings suggest a potential involvement of ephrin-Eph signaling in tonotopic map formation.

To further explore if ephrins and Ephs are involved in tonotopic map formation in the central auditory system, we began with an expression screen of the ephrin-A subclass members. We found that ephrin-A3 molecules show differential expression along the tonotopic axis in the CN and repel growing ANFs in a stage-dependent manner. In mice lacking the ephrin-A3 gene, they show a degraded tonotopic map, altered auditory activation patterns, and impaired detection of sound frequency changes. These results establish an essential role for ephrin-A3 in tonotopic map formation in the CN.

2 | MATERIALS AND METHODS

2.1 | Mice

All animal experiments in this study have been performed in compliance with institutional and National Institutes of Health guidelines approved by the Institutional Animal Care and Use Committee at Loyola University Chicago (Protocol 1926). All efforts were made to minimize the number of mice used and their suffering. The ephrin-A3 knockout (*Efna3*$^{-/-}$) mouse strain was obtained from the Jackson Laboratory (Stock Number: 019108) and has been described and validated previously (Carmona et al., 2009). Mice were maintained on the C57/BL6 background. Breeding pairs used were male and female mice heterozygous for the ephrin-A3 knockout allele (*Efna3*$^{+/-}$). *Efna3*$^{-/-}$ mice were PCR genotyped using the EphrinA3.F forward primer (5′-TGT GGG CGT GAC TAA GAT TG-3′), the E1.R reverse primer (5′-CAC TGC TGA TTG GAG CTG TTC-3′), and the YFP.R reverse primer (5′-GAA CTT CAG GGT CAG CTT GC-3′) (wt, 250 bps; ephrin-A3 knockout allele, 350 bps). Both male and female mice were used in the experiments. In most experiments, wild-type (*Efna3*$^{+/+}$) gender-matched littermates were used as controls. In rare occasions, heterozygous (*Efna3*$^{+/-}$) gender-matched littermates were used as controls due to the lack of wild-type animals in the litter. For timed pregnancies, male and female mice were put together at 5 p.m. and checked for the presence of a vaginal plug the following morning at 9 a.m. Plugs were assumed to occur at midnight so noon on the day of a plug was defined as embryonic day 0.5 (E0.5).

2.2 | RNAScope in situ hybridization

E15.5 and E17.5 CD1 mouse heads were fixed directly in 4% paraformaldehyde (PFA) in phosphate-buffered saline (PBS) overnight at 4°C. Embryo heads were stepped through 10, 20, and 30% sucrose in PBS, and embedded in NEG50 (Richard-Allan Scientific). Coronal head sections through the cochlea and the CN were prepared at 20 μm. In situ hybridization was performed according to the protocols of the RNAscope 2.5 HD Duplex Assay, the RNAscope 2.5 HD Assay – RED, or the RNAScope Multiplex Fluorescent V2 Assay (Advanced Cell Diagnostics). The signals were detected using a horseradish peroxidase (HRP)-based chromogenic assay (blue signals), an alkaline phosphatase (AP)-based chromogenic assay (red signals), or an HRP-based Opal fluorophore assay (Opal 520, Opal 570, and Opal 690) (Akoya Biosciences).

Probes used were *Efna1* (Cat No. 428621), *Efna2* (Cat No. 507481-C2), *Efna3* (Cat No. 473971), *Efna4* (Cat No. 487621-C2), *Efna5* (Cat No. 316641-C2), *Mafb* (Cat No. 438531-C2), *Atoh1* (Cat No. 408791-C3), *c-fos* (Cat No. 316921), *EphA4* (Cat No. 419081), and *EphA7* (Cat No. 458661). A negative control probe (*Escherichia coli DapB*, Cat No. 310043) and a positive control probe (mouse *Ppib*, Cat No. 313911) were also included in the procedure to ensure that the assay was performed properly. Because the NeuN staining was not possible after the target retrieval procedure, we used DAPI (Thermo Fisher Scientific, 62248) or a rabbit anti-TuJ1 antibody (BioLegend, 802001, RRID: AB_2564645) to counterstain the tissues to reveal the cellular structure or to mark the embryonic CN or the SGNs at the end of the in situ hybridization protocol. Tissue sections were blocked for 1 h at room temperature in PBS containing 5% normal goat serum and 0.3% Triton X-100. Sections were then stained with

the rabbit anti-TuJ1 antibody diluted in the blocking solution overnight at 4°C, followed by Alexa Fluor-conjugated secondary antibodies (Thermo Fisher Scientific) at RT for 1 h, and mounted in Fluoromount-G (Southern Biotech, 0100-01). Images were acquired on a Nikon Eclipse Ni-U microscope using a Plan Apo λ 4× (NA:0.2) or a Plan Fluor 10× (NA:0.3) objective, or on an Olympus FluoView FV1000 using a 100× (NA:1.40) oil-immersion objective.

For quantification of *Efna3* RNAScope Signals in the VCN/AVCN, the RNAScope images were converted to grayscale images in ImageJ (National Institutes of Health). Thresholds were set using the "Auto Threshold" function by the default algorithm of the ImageJ. The areas of the VCN/AVCN were equally divided in half along the ventral to dorsal axis as the ventral and the dorsal regions. The average intensity of RNAScope Signals in the ventral and dorsal halves of the VCN/AVCN were analyzed by measuring the mean gray value using ImageJ and the values were compared by the Welch's unequal variances *t* test.

2.3 | Ephrin-A3 stripe assay

Stripe assays were conducted as described previously (Knöll et al., 2007; Treffy et al., 2016). Briefly, 22-mm coverslips were first coated with poly-D-lysine (MilliporeSigma, P7280) at 0.1 mg/ml for 2 h at 37°C, rinsed twice with deionized water, sterilized with 70% ethanol, and air-dried. For experimental coverglasses, first stripe solutions contained 2–40 μg/ml recombinant ephrin-A3-Fc chimera protein (R&D Systems, 359-EA-200) (human IgG-Fc was added together with 2–20 μg/ml ephrin-A3-Fc to fill in the concentration to 40 μg/ml). For control coverglasses, first stripe solutions contained 40 μg/ml human IgG-Fc (MilliporeSigma, AG714). The chimera proteins or IgG-Fc were preclustered for 30 min on ice with 5 μg/ml Alexa Fluor 488 goat anti-human antibody in Hanks' balance salt solution (HBSS, Thermo Fisher Scientific). For the second stripe solution, 40 μg/ml human IgG-Fc was preclustered as above but with 5 μg/ml unconjugated goat anti-human Fc (MilliporeSigma, AP113). Silicon manifolds with 90-μm channels purchased from Dr Martin Bastmeyer (Knöll et al., 2007) were applied to polylysine-treated coverglasses. Total volume of 100 μl of the first stripe solution was put into the matrices and incubated for 30 min at 37°C. After washing three times with HBSS, the matrices were removed and 100 μl of the second stripe solution was applied and incubated for 30 min at 37°C to coat the unbound region between the first stripes. After three more washes with HBSS, the coverslips were incubated overnight at 4°C in 100 μl of HBSS containing 2.5 μg/ml laminin (BD Biosciences, 354232), followed by three washes with HBSS.

E15.5 or E17.5 CD1 cochleae were dissected out under sterile conditions. Cochlear explants were prepared by using a one-third turn of the cochlea from either the most basal aspect or the most apical aspect of the cochlea (cochleae from these stages contain about two full turns). Explants were plated on the coverslips in 100 μl serum-free Neurobasal medium (21103049) containing 1.4 mM L-glutamine (25030149), N2 supplement (17502048, all from Thermo Fisher Scientific), 10 ng/ml BDNF (ProSpec, CYT-207), and 10 ng/ml NT-3 (ProSpec, CYT-688), and cultured for 36–48 h at 37°C with 5% CO_2.

For staining, explant cultures were fixed with 4% PFA in 0.1 M sodium cacodylate, pH 7.4 (Electron Microscopy Sciences, 11650) containing 10 mM $MgCl_2$ and 5 mM $CaCl_2$ for 12 min and washed with 0.1 M cacodylate buffer followed by PBS. Explants were blocked for 1 h at room temperature in PBS containing 1% tween-20, 5% DMSO, 1% fish gelatin, and 1.4 mg/ml BSA (PBSTD, all from MilliporeSigma), followed by a 1-h incubation in mouse anti-neurofilament (Developmental Studies Hybridoma Bank, 2H3, RRID: AB_531793); mouse anti-GAP43 (MilliporeSigma, MAB347, RRID: AB_94881); and rabbit anti-Myosin-VI (Proteus BioSciences, 25-6791, RRID: AB_2314836). Explants were washed three times in PBSTD, incubated in Alexa Fluor-conjugated secondary antibodies at RT for 40 min, washed three times again in PBSTD, and mounted in Fluoromount-G. Confocal images were obtained on an Olympus FluoView FV1000 using a XL Fluor 4×/340 (NA:0.28) or a 10× (NA:0.40) objective, or a 60× (NA:1.40) oil-immersion objective. A 1600 × 1600 image was acquired at the optimal step size (automatically calculated by the Olympus software) in the z axis.

For quantitative evaluation of ephrin-A3 repulsion, stripes were oriented vertically, and outgrowth of ANFs was divided into quadrants. We measured the longest ANF outgrowth that was continuous in the labeled stripes (stripes containing 0–40 μg/ml ephrin-A3-Fc) within the upper and lower quadrants (i.e., approximately parallel to the stripes) for each explant, and took the ratio of that value to the length of the longest ANFs in the unlabeled stripe (stripes containing no ephrin-A3-Fc) for the same explant. Multiple ANFs were considered in each stripe and the most common length of the longest three to five ANFs were used. ANFs that crossed over into different stripes were disregarded. Statistical significance between test groups was assessed by three-way ANOVA with post hoc Welch's unequal variances *t* test.

2.4 | NeuroVue labeling from the cochlea to the AVCN

E18.5 mouse heads were fixed directly in 4% PFA in PBS overnight at 4°C and rinsed in PBS. The tissues on the ventral side of the head were removed to expose the cochlea. The cochlea was further dissected to reveal the basal and apical turns. NeuroVue labeling was performed as described previously (Karmakar et al., 2017). Small incisions were created using a Dumont #5 super fine forceps (Fine Science Tools, 11252-00) at a location between the middle and basal turns and at the apical turn. Special care was taken to make sure that the incisions were made around the same position of the cochlea for each sample. Triangular nylon filter paper strips (approximately 250 μm × 250 μm × 150 μm each) coated with distinct NeuroVue dyes (Molecular Targeting Technologies, Red FS-1002 or Maroon FS-1001) were inserted into the incisions at the different turns of the cochlea. The heads were incubated in 4% PFA in PBS at 37°C for 10 days. The brain was dissected out and embedded in 4% low

melting agarose (IBI Scientific, IB70056) in PBS. Then, 60 μm vibratome sections anterior to the eighth nerve root were identified as the AVCN and collected. The dissected cochlea and AVCN sections were counterstained with an anti-NeuN antibody (Abcam, ab177487, RRID: AB_2532109) and mounted in Fluoromount-G. Confocal images were obtained on an Olympus FluoView FV1000 using a 4×/340 (NA:0.28, for the cochlea) or a 10× (NA:0.40, for the AVCN) objective at the optimal Z-step size. ImageJ was used to calculate areas in the AVCN and to measure the areas of the NeuroVue-labeled spiral ganglion in the cochlea. sg_{mb} or sg_a is the area of the dye-labeled spiral ganglion in the mid-basal or apical cochlear turn. S_{mb} or S_a is the AVCN area innervated by NeuroVue-labeled ANFs from the mid-basal or the apical cochlear turn. S_{AVCN} is the total AVCN area. For measurement of S_{mb}, S_a, and S_{AVCN}, the section containing the largest S_{AVCN} was chosen for analysis in each animal. The AVCN border was demarcated from the small granule cell region according to the NeuN staining. The fraction of AVCN area innervated by dye labeled ANFs from the mid-basal or apical turn were calculated as ($S_{mb}/S_{AVCN} \times 100$) or ($S_a/S_{AVCN} \times 100$) respectively and normalized to sg_{mb} or sg_a. The distance between S_{mb} and S_a was measured using ImageJ and normalized to the total length of the dorsal-ventral axis of the corresponding AVCN. The values obtained from the control and *Efna3*$^{-/-}$ mutant mice were then compared using the Welch's *t* test.

2.5 | *c-fos* induction assay after pure tone stimulation

c-fos activation after pure tone stimulation was performed as described previously (Karmakar et al., 2017; Miko et al., 2007). Freely moving 5- to 7-week-old mice were placed inside a custom-made cylinder enclosure (14 cm diameter × 15 cm height) built using stainless steel wire mesh. The mice in the enclosure were kept in silence in an anechoic chamber (Med Associates, ENV-022SD) for an hour, followed by exposure to free field tone pips (16 kHz and/or 8 kHz) at 75 dB sound pressure level (SPL) for 90 min. Tones were delivered using a RZ6 Multi-I/O processor (Tucker-Davis Technologies) with a Crown DCi 2|300 power amplifier and a Pyramid TW57 speaker. The speaker was mounted on the top of the cylinder enclosure and positioned approximately 10 cm above the mouse head. Stimuli were calibrated using a ¼ in. free-field microphone (PCB Piezotronics, 378C01). One group of animals were exposed to 16 kHz tone pips (400 ms duration, with a 5 ms rise-fall time and 300 ms gap, presented at 1.43 Hz frequency) for 90 min. One group of animals were exposed to 8 kHz tone pips (50 ms duration, with a 4 ms rise-fall time and 40 ms gap, presented at 11.1 Hz frequency) for 90 min. The third group of animals was exposed to alternating 8 kHz (400 ms, 1.43 Hz) and 16 kHz (400 ms, 1.43 Hz) dual tones for 90 min. The acoustic stimuli were composed using the RPvdsEx software (Tucker-Davis Technologies). Immediately after tone exposure, animals were transcardially perfused with ice-cold PBS, followed by 4% PFA in PBS. Brains were postfixed in 4% PFA in PBS for 24 h at 4°C, stepped through the sucrose gradient and embedded as described above, and coronal brain sections through the AVCN were prepared at 40 μm. *c-fos* activation was detected by in situ hybridization using RNAscope 2.5 HD Assay – RED as described above.

For quantification, the area covered by the *c-fos*-positive cells or the separation area between two activated isofrequency bands upon dual-tone exposure, and the total AVCN area were measured blind to the genotype using the ImageJ. The section containing the largest AVCN area was chosen for analysis in each animal. The AVCN border was demarcated from the small granule cell region based on the DAPI staining. The percentage of *c-fos*-positive area in the AVCN or the percentage of the area between the two *c-fos*-positive bands in the AVCN was calculated and compared between the control and *Efna3*$^{-/-}$ mutant animals using the Welch's *t* test.

2.6 | Immunohistochemistry

Immunohistochemistry of tissue sections and whole mount cochleae were performed as previously described (Yu et al., 2013). Briefly, sections of cochleae or CN were blocked for 1 h at room temperature in a solution containing 5% normal donkey serum and 0.3% Triton X-100 in PBS. Samples were then incubated overnight at 4°C in primary antibodies diluted in the blocking solution, followed by Alexa Fluor-conjugated secondary antibodies at room temperature for 1 h. For cochlear whole-mount staining, fixed cochleae were dissected into three pieces corresponding to the apical, middle, and basal turns. The microdissected pieces were blocked in PBS with 1%Triton X-100 and 5% normal donkey serum for 1 h at room temperature and then incubated in primary antibodies diluted in blocking solution at 37°C for 20 h. Alexa Fluor-conjugated secondary antibodies were used for signal detection. Primary antibodies used were the rabbit anti-NeuN antibody (Abcam, ab177487, RRID: AB_2532109), the rabbit anti-TuJ1 antibody (BioLegend, 802001, RRID: AB_2564645), the guinea pig anti-parvalbumin (Synaptic Systems, 195 004, RRID: AB_2156476), the rabbit anti-vesicular acetylcholine transporter (Synaptic Systems, 139 103, RRID: AB_887864), and the guinea pig anti-choline acetyltransferase (Synaptic Systems, 297 015, RRID: AB_2744644).

2.7 | Auditory brainstem response recordings

Here, 5- to 7-week-old mice were anesthetized with ketamine (1 mg/10 g body weight IP injection, Patterson Veterinary, 07-893-5790) and xylazine (0.1 mg/10 g body weight IP injection, Patterson Veterinary, 07-891-9200). Needle electrodes (Tucker-Davis Technologies, ELE-N) were inserted subdermally at the vertex of the skull (recording electrode), the lower region below the stimulated ear (reference electrode), and the hind hip of the animal (ground electrode). Auditory brainstem response (ABR) recordings were conducted inside the Med Associates anechoic chamber using an open field setup. A MF1 Multi Field Magnetic speaker (Tucker-Davis Technologies) was placed 10 cm from the subject's ear and positioned

in line with the axis of the ear canal. Stimulation protocols of tone bursts were programmed in the SigGenRZ software and presented using the BioSigRZ software (both from Tucker-Davis Technologies). ABR recordings were conducted using tone pips at 5.6, 8, 11.3, 16, 22.6, 32, and 45.2 kHz (2.5 ms in duration with a 0.2 ms rise/fall time presented at a rate of 21 Hz) in 5 dB steps from below threshold to 90 dB SPL as described previously (Yu et al., 2013). The voltage difference between the recording and the reference electrodes was amplified, filtered, digitized, and averaged across 512 presentations in the BioSigRZ. Wave amplitudes and latencies of ABRs were extracted from the BioSigRZ. Threshold was defined by visual inspection of stacked waveforms. Statistical significance was analyzed using two-way ANOVA with post hoc Welch's *t* test.

2.8 | Acoustic startle response-based assays for evaluating frequency discrimination

Acoustic startle response (ASR)-based procedures of assessing frequency discrimination in mice were conducted as described previously (Clause et al., 2011; Clause et al., 2017; Mwilambwe-Tshilobo et al., 2015) using a semi-custom-made setup. The audio files were programmed using the Audacity software and saved as waveform audio files. Auditory stimulation was delivered through an ADI-2 Pro FS AD/DA Converter (RME Audio) with a Crown DCi 2|600 amplifier and a TL16H super tweeter speaker (VISATON, 200 W peak, frequency response: 2.2–35 kHz). The TL16H tweeter was used because it has a very flat response from 5 to 20 kHz and a uniformly distributed energy pattern. Auditory stimuli were calibrated by the REW acoustics analysis software using the PCB 378C01 ¼ in. free-field microphone placed at the level of the subject's ear within an animal holder (Med Associates, ENV-263A) in the anechoic chamber. Animals were habituated for 4 days prior to the test. On the first day, the animal holder was placed inside each mouse cage. On the second day, each animal was placed in the holder for 25 min inside the anechoic chamber. On the third and fourth days, a 16 kHz background tone at 70 dB SPL was presented to the animal for 25 min from the TL16H tweeter placed 10 cm in front of the animal. At the beginning of the assay, animals in the holder were allowed to acclimate to the 16 kHz background tone (F1 tone) at 70 dB SPL for 5 min, followed by startle-only and prepulse trials. The sequences of the trials were composed using the Advanced Startle software (Med Associates, SOF-828) and contained three parts. The first part consisted of a series of startle-only trials for short-term habituation. The second part comprised prepulse trials randomly mixed with an equal number of startle-only trials. Seven prepulse frequencies (F2 tones) used were 15.92 kHz (0.5% change), 15.68 kHz (2% change), 15.47 kHz (3.3% change), 15.2 kHz (5% change), 14.4 kHz (10% change), 13.34 kHz (16.6% change), and 12 kHz (25% change). The third part was made up of a serial of startle-only trials again to assess habituation during the course of the assay. In prepulse trials, the prepulse stimulus contained a frequency change of a linear rise-fall of 1 ms from the background F1 tone to the prepulse F2 tone at 70 dB SPL. F2 tone was maintained for 80 ms in the interstimulus interval, followed by the startle stimulus of a white noise burst at 120 dB SPL for 40 ms (Figure 10(a–e)). After the startle stimulus, F1 background tone was given again until the prepulse stimulus of the next trial. For startle only trials, the prepulse stimulus comprised a linear rise-fall of 1 ms from F1 tone to F1 tone without actually introducing a frequency change. All trials were separated randomly by an interval range from 10 to 20 s. The vertical force exerted by the animal was recorded on a platform load cell assembly with an amplifier (Med Associates, PHM-255A and PHM-250B) and acquired and digitized by a PCI Data Acquisition Card and an A/D interface (Med Associates, DIG-744 and ANL-729) using the Advanced Startle software. All mice were monitored during the assay by a USB infrared webcam (Ailipu Technology, ELPUSBFHD01M). Two 500-ms periods were recorded in each trial (Figure 10(a)). The baseline activity was recorded in the first 500-ms period, which happened immediately before the prepulse. The ASR was recorded in the second 500-ms period, which started at the onset of the startle stimulus. Both the positive and negative directions of the maximum force were recorded and reported as the ASR. The recording traces were exported and analyzed in the Microsoft Excel. Statistical significance was assessed using two-way ANOVA with post hoc Welch's *t* test.

2.9 | Statistics

All statistical analyses were carried out in Microsoft Excel and GraphPad Prism to determine if sets of data are significantly different from each other. The difference between means was considered significant if $p < .05$. Data were plotted using GraphPad Prism. The results are expressed as means ± *SD*s unless otherwise noted.

3 | RESULTS

3.1 | Ephrin-A3 molecules are differentially expressed along the tonotopic axis in the developing CN

Expression patterns of ephrin-A members were determined in the CN during the emergence of tonotopic maps at E15.5 and E17.5. Because cell surface molecules, such as ephrins and Ephs, are sometimes expressed at low levels, we used RNAScope in situ hybridization, a procedure that allows us to detect expression of low-abundance RNA transcripts semiquantitatively.

At E15.5, the CN anlage is still quite immature as DCN cells continue to proliferate and the DCN is fully caudal to the VCN. Shortly after this stage, the hindbrain flexes, resulting in the DCN shifting dorsal to the VCN (Farago et al., 2006). By analyzing expression of *Efnas* in the CN anlage on E15.5 and E17.5, we found that *Efna1* is not expressed in the CN and *Efna4* is expressed in the eighth nerve root but not inside the CN (Figure 1(a,b,g,h); VCN anlage shown on E15.5 and AVCN anlage shown on E17.5 in all panels). *Efna2* and *Efna5* are

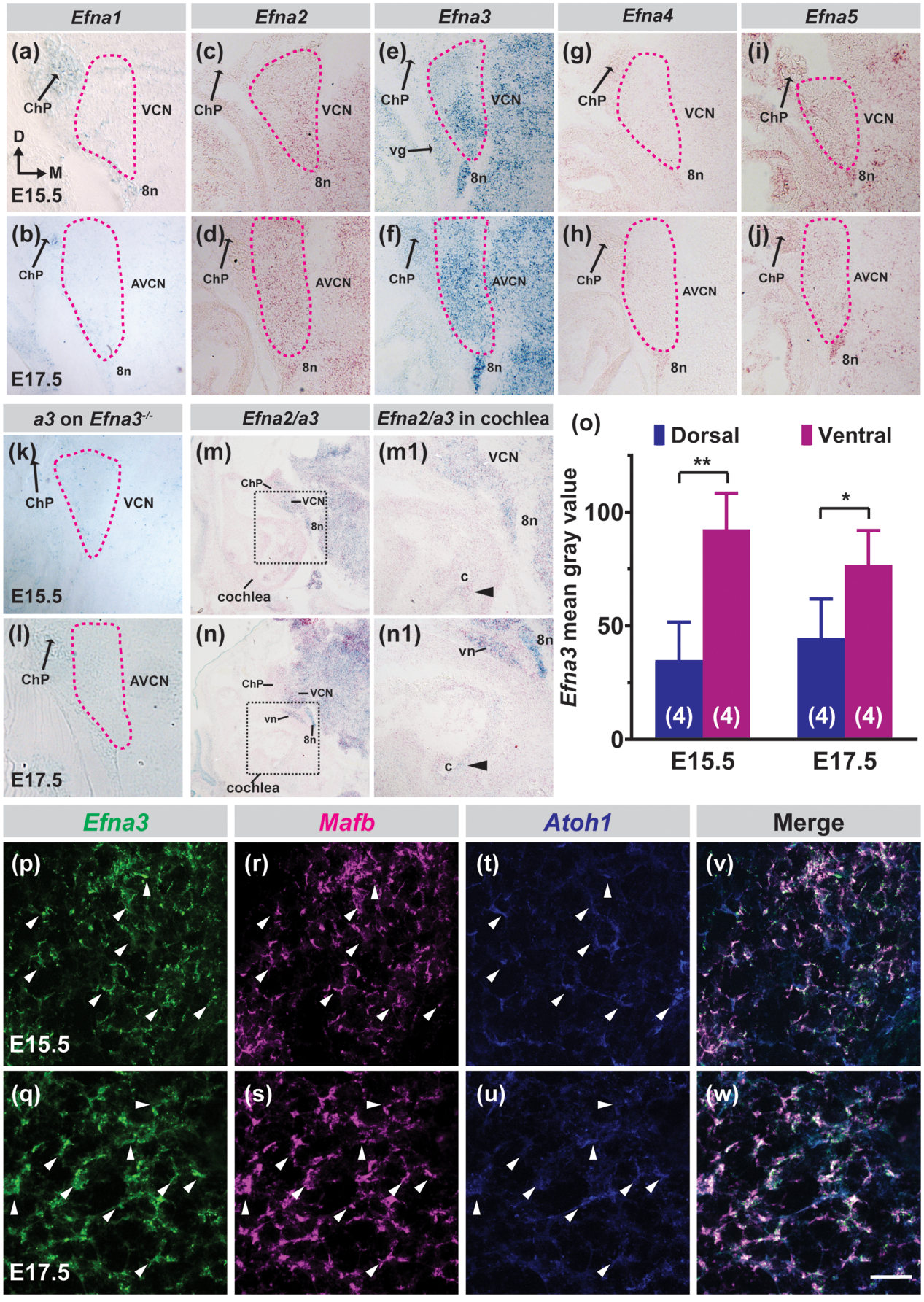

FIGURE 1 Legend on next page.

expressed at lower levels in the CN anlage (Figure 1(c,d,i,j)). *Efna3* expression is particularly interesting. *Efna3* is differentially expressed along the tonotopic axis in the CN anlage, with future lower-frequency regions showing greater expression than future higher-frequency regions (Figure 1(e,f)). Quantification of *Efna3* RNAScope Signals in the ventral and dorsal regions of the VCN/AVCN showed that *Efna3* was differentially expressed along the ventral to dorsal axis in the developing VCN/AVCN, with higher *Efna3* expression in the ventral than in the dorsal regions (Figure 1 (o)). No *Efna3* expression signals were detected in *ephrin-A3*$^{-/-}$ CN anlage (Figure 1(k,l)), confirming the specificity of *Efna3* probes. Moreover, *Efna3* expression was found to be predominantly expressed by Atoh1-derived Mafb-positive bushy cells (Fujiyama et al., 2009; Saul et al., 2008), the output neurons of the AVCN (Figure 1(p–w)). We also observed that *Efna3* is expressed at a very low level in the cochlea when compared to its expression in the CN at these stages (Figure 1(m–n1)), so we decided to focus our studies first on the role of ephrin-A3 forward signaling (ephrin-A3 ligands in CN activating Eph receptors in SGN afferents) during tonotopic map formation in the CN.

3.2 | EphA receptors are expressed in developing SGNs

Ephrin-As primarily interact with EphA receptors to activate forward signaling. Ephrin-A3 is known to bind to all 10 EphAs with different binding affinities (Egea & Klein, 2007). To determine potential EphA receptors in SGNs which could mediate ephrin-A3 forward signaling in the CN, we performed a pilot RNA-Seq experiment to detect which EphA receptors are expressed at high levels in E16.5 cochleae. Of the 10 EphAs, *EphA4* and *EphA7* are expressed at the high levels, with a Fragments Per Kilobase of transcript per Million mapped reads (FPKM) value greater than 10 (Table 1: *EphA4*: 12.76 FPKM, *EphA7*: 41.92 FPKM from one pilot RNA-seq experiment of extracts from eight cochleae). To assess whether *EphA4* and *EphA7* are expressed in developing SGNs, we conducted RNAScope in situ hybridization in E15.5 and E17.5 cochleae.

EphA4 was broadly expressed in many regions of the cochlea at these stages, including mesenchyme, the cochlear epithelium, and the spiral ganglion (Figure 2(a,a1,c,c1)). *EphA7* exhibited high expression in the cochlear epithelium and moderate expression in the spiral ganglion at E15.5 and E17.5 (Figure 2(b,b1,d,d1)). These results are consistent with previous observations (Coate et al., 2012; Kim et al., 2016). The spatially and temporally complementary expression of *EphA4* and *EphA7* in SGNs and *Efna3* in CN are consistent with ephrin-A/EphA forward signaling playing a role in targeting of SGN afferents in the developing CN.

3.3 | Ephrin-A3 forward signal repels ANFs in a developmental stage-dependent manner

Since the ephrin-A3 gene shows an intriguing expression pattern in the CN and potential EphA receptors are expressed in SGNs during development, we developed an ephrin-A3 stripe assay using cochlear ganglion explants to determine whether ephrin-A3 molecules are sufficient to guide growing ANFs at the time they would be innervating the CN.

E15.5 and 17.5 mouse cochleae were isolated and divided into pieces to establish the explants. To compare whether ANFs from the base and the apex of the cochlea have different responses to ephrin-A3, we prepared a one-third turn of the cochlea from either the most basal (contain mostly future high-frequency SGNs) or the most apical aspect (contain mostly future low-frequency SGNs) of the cochlea. To allow us to distinguish peripheral processes of SGNs from their central processes and to help us better orient the cochlear ganglion explants, we preserved the sensory epithelium in our explant culture system and used myosin VI staining to mark the developing auditory hair cells. At E15.5, hair cells just start to differentiate so myosin VI antibodies only label inner hair cells in the base but not the apical inner hair cells nor all outer hair cells. By E17.5, one row of inner hair cells and three to four rows of outer hair cells could be visualized by myosin VI staining in all regions of the cochlea (Figure 3(a,b)). In our explant culture system, we used neurofilament/GAP43 staining to reveal growing ANFs and found that the peripheral processes of ANFs were still

FIGURE 1 Expression of *Efnas* in the E15.5 or E17.5 mouse cochlear nucleus (CN) and cochleae. (a–l) The expression levels of *Efnas* in the CN were detected by RNAScope in situ hybridization using a horseradish peroxidase (HRP)-based chromogen (blue) or an alkaline phosphatase (AP)-based chromogen (red). Only VCN or anteroventral cochlear nucleus (AVCN) are shown and outlined with magenta dashed lines. (a,b,g,h) *Efna1* and *Efna4* are not expressed inside the CN. (c,d,i,j) *Efna2* and *Efna5* are expressed at lower levels in the developing VCN/AVCN. (e,f) *Efna3* is differentially expressed along the tonotopic axis in the developing VCN/AVCN. (k,l) The specificity of *Efna3* probes was validated by a negative signal on sections from *Efna3*$^{-/-}$ mice. (m–n1) The expression of *Efna2* and *Efna3* in the cochlea and CN was detected by RNAScope in situ hybridization using an HRP-based chromogen (blue) or an AP-based chromogen (red). Compared to *Efna2* expression (red signals), *Efna3* (blue signals) is expressed much higher in the CN than in the cochlea at E15.5 and E17.5. (m1) and (n1) are the high magnification of the boxed regions in (m) and (n). *Efna3* is not expressed in most regions in the cochlea except at a low level near the cochlear duct. ChP, choroid plexus of the fourth ventricle; 8n, eighth nerve; vn, vestibular nucleus; c, cochlear duct. The axis in (a) indicates the orientation of all the sections in the figure. D, dorsal; M, medial. (o) Quantification of RNAScope Signals of *Efna3* in the ventral and dorsal regions of the VCN/AVCN shows that *Efna3* is differentially expressed along the ventral to dorsal axis in the developing VCN/AVCN. (p–w) Expression of *Efna3*, *Mafb*, and *Atoh1* were detected by RNAScope multiplex in situ hybridization in VCN cells using HRP-based Opal fluorophores (*Efna3*: Opal 520 [green], *Mafb*: Opal 570 [pseudo-colored magenta], and *Atoh1*: Opal 690 [pseudo-colored blue]). *Efna3* expression was found in cells expressing *Mafb* and *Atoh1* (i.e., bushy cells, arrowheads) in the VCN. Scale bar: 200 μm (a–l,m1,n1); 500 μm, (m,n); or 24 μm (p–w) [Color figure can be viewed at wileyonlinelibrary.com]

Gene name	Transcription start site (tss_id)	Chromosomal location	FPKM
EphA1	TSS19981	chr6:42358486–42373268	4.40
EphA2	TSS22389	chr4:141301220–141329384	0.73
EphA3	TSS19153	chr16:63545217–63864157	7.59
EphA4	TSS26846	chr1:77367184–77515088	**12.76**
EphA5	TSS1648	chr5:84054764–84417382	2.13
EphA6	TSS4926	chr16:59653482–60605531	0.08
EphA7	TSS10732,TSS21355	chr4:28813130–28967503	**41.92**
EphA8	TSS21385	chr4:136929418–136956816	0.20
EphA10	TSS26448	chr4:124881784–124917800	0.24

TABLE 1 Expression levels of *EphA* receptors in FRKM

Bold values are significance.
Abbreviation: FPKM, Fragments Per Kilobase of transcript per Million mapped reads.

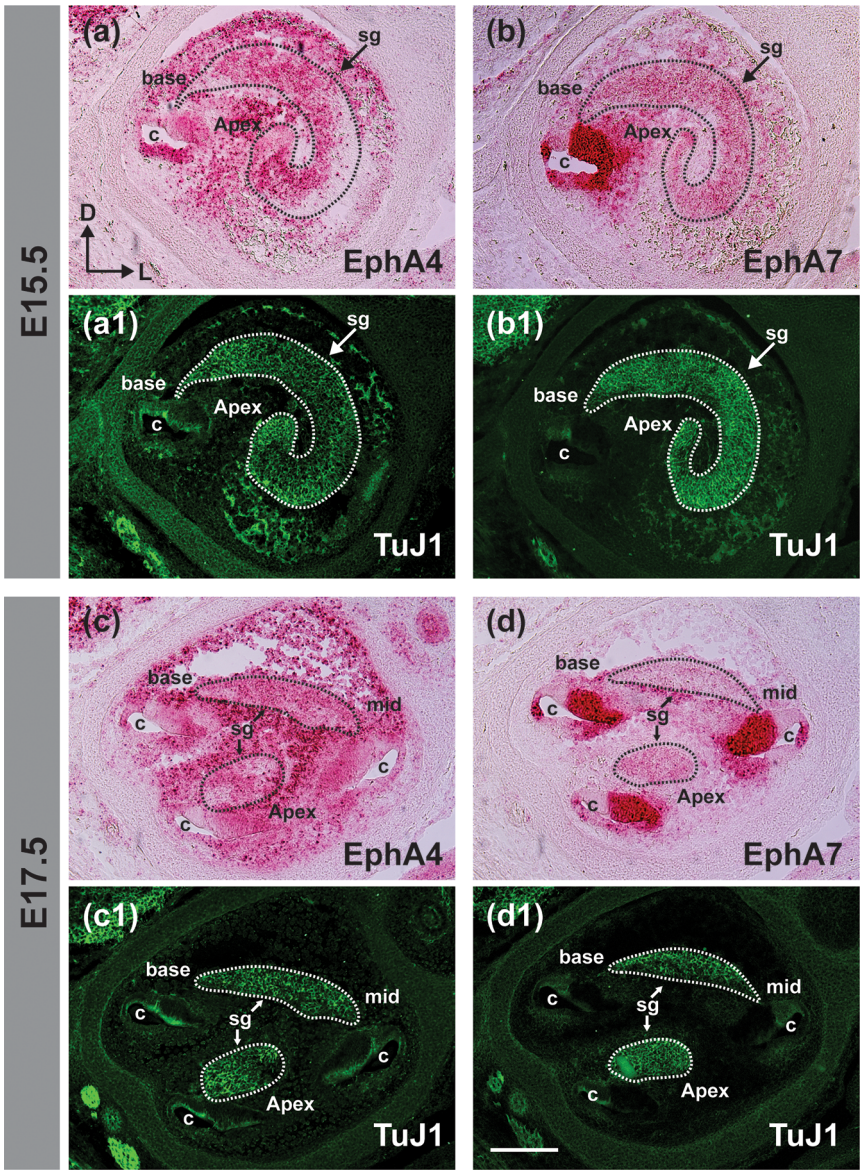

FIGURE 2 EphA receptors are expressed in developing spiral ganglion neurons (SGNs). (a–d1) Expression of *EphA4* and *EphA7* receptors in E15.5 or E17.5 cochleae were detected by RNAScope in situ hybridization using an alkaline phosphatase (AP)-based chromogen (red). The cochlear sections were co-stained with TuJ1 to mark the spiral ganglion (sg, green). The spiral ganglion was outlined with dashed lines based on TuJ1 staining. Both *EphA4* and *EphA7* receptors are expressed in developing SGNs. c: cochlear duct. The axis in (a) indicates the orientation of all the sections in the figure. D, dorsal; L, lateral. Scale bar: 200 μm [Color figure can be viewed at wileyonlinelibrary.com]

preserved, but their staining intensity is much weaker than the intensity of central processes. Peripheral processes can only be visualized at a magnification higher than 600× as shown in Figure 3(b). This allows us to easily distinguish the central processes of ANFs from their peripheral processes with confidence and use this system to test the responses of growing ANFs in the CN to ephrin-A3.

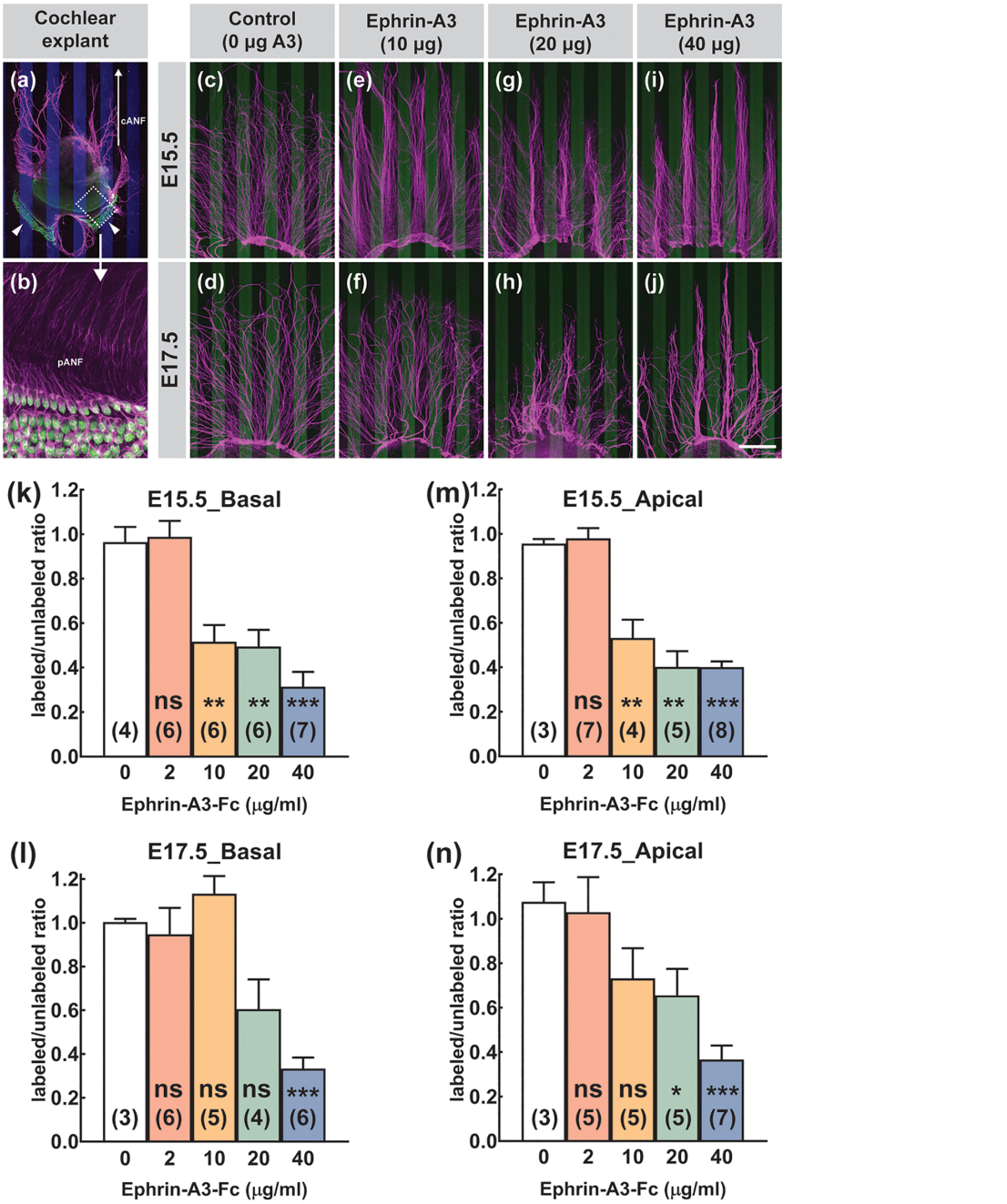

FIGURE 3 Ephrin-A3 forward signaling repels central processes of auditory nerve fibers (ANFs) in a developmental stage-dependent manner. (a,b) An explant from the E17.5 basal cochlear turn was cultured on the stripes containing preclustered ephrin-A3-Fc (40 µg/ml, shown in pseudo-colored blue) for 36 h, and stained with anti-Myosin-VI to mark the developing hair cells (green, arrowheads in a) and anti-neurofilament/GAP43 to reveal growing ANFs (magenta). (b) It is the high magnification of the boxed region in (a). In this culture system, the peripheral processes of ANFs are still preserved but their staining intensity is much weaker than the intensity of the central processes. Peripheral processes can only be visualized at a magnification higher than 600× as shown in (b). This allows us to distinguish ANF central processes on the stripes from their peripheral processes. cANF or pANF: the central or peripheral processes of ANFs. (c–j) Explants from E15.5 or E17.5 apical cochlear turns cultured on the stripes containing different concentrations of preclustered ephrin-A3-Fc. In control cultures, both stripes contained preclustered unconjugated human-IgG Fc (40 µg/ml) but the first stripe was preclustered with an Alexa-488-goat antihuman IgG-Fc (green stripes) whereas the second stripe was preclustered with an unlabeled goat antihuman IgG-Fc (uncolored stripes). In ephrin-A3 cultures, the first stripe contained 10, 20, or 40 µg/ml ephrin-A3-Fc preclustered with an Alexa-488-goat antihuman IgG-Fc (green stripes) and the second stripe (uncolored) was the same as in control cultures. No bias is observed in control cultures (c,d). ANFs show a developmentally reduced response to ephrin-A3. At E15.5, ANFs were already strongly repelled by stripes containing 10 µg/ml ephrin-A3-Fc (e,g,i). In contrast, E17.5 ANFs can only be strongly repelled by stripes when ephrin-A3-Fc concentration was increased to 40 µg/ml (f,h,j). Scale bar: 600 µm (c–j), 240 µm (a), and 40 µm (b). (k–n) Statistics of stripe assays indicates that ANFs show a developmentally reduced sensitivity to ephrin-A3. At E15.5, both apical and basal ANFs were strongly repelled by 10 µg/ml ephrin-A3-Fc stripes. At E17.5, basal ANFs only showed repulsion to 40 µg/ml ephrin-A3-Fc stripes. Apical ANFs showed weak repulsion to 20 µg/ml ephrin-A3-Fc stripes and repulsion to 40 µg/ml ephrin-A3-Fc stripes. Numbers on the bar indicate the sample size. Means ± *SD*s are shown. ns: not significant, $^{*}p < .05$, $^{**}p < .01$, $^{***}p < .001$, three-way ANOVA with post hoc Welch's *t* test [Color figure can be viewed at wileyonlinelibrary.com]

Control coverglasses were coated with alternating stripes of Alexa Fluor 488-labeled and unlabeled human IgG-Fc. ANFs from basal or apical cochlear ganglia obtained at E15.5 or E17.5 showed no preference for either stripe on control coverglasses (Figure 3(c,d)). On the experimental coverglasses, ANFs from E15.5 ganglia were emitted in parallel to ephrin-A3 stripes and grew significantly less on the ephrin-A3-Fc stripes than control stripes if 10, 20, and 40 μg/ml ephrin-A3-Fc, but not 2 μg/ml ephrin-A3-Fc, were used to prepare the test stripe (Figures 3(e,g,i,k,m) and 4 for statistical analyses). We also found that ANFs from basal and apical ganglia exhibited a comparable response to ephrin-A3 repulsion (Figures 3(k,m) and 4). Since basal and apical ANFs were similarly repelled by ephrin-A3 forward signaling, we provide representative images only from experiments of the apical ganglia (Figure 3(c–j)). On the experimental coverglasses using E17.5 cochlear explants, ANFs showed a decreased response to ephrin-A3 repulsion. E17.5 ANFs were no longer repelled by stripes containing 10 μg/ml ephrin-A3-Fc and could only be repelled by stripes containing 40 μg/ml ephrin-A3-Fc (Figures 3(f,h,j,l,n) and 4). Again, both basal and apical ANFs from E17.5 cochlear ganglia demonstrated a similar developmentally reduced response to ephrin-A3 repulsion, although the response was reduced more in basal than in apical ANFs (Figures 3(l,n) and 4). Apical but not basal ANFs could still be moderately repelled by stripes containing 20 μg/ml ephrin-A3-Fc (Figure 3(n)). Statistical analyses were used to compare the ephrin-A3 repulsive responses between ANFs from basal and apical ganglia and between ANFs from E15.5 and E17.5 ganglia. ANFs from basal and apical ganglia showed no significant difference in their responses to ephrin-A3 repulsion (three-way ANOVA, basal vs. apical, $F_{(1,85)} = 0.1738$, $p = .68$; Figure 4). The developmental stage-dependent change in sensitivity to the repulsive influence of ephrin-A3-Fc stripes was significant, the E15.5 ANFs were more sensitive than the E17.5 ANFs (three-way ANOVA, E15.5 vs. E17.5, $F_{(1,85)} = 11.24$, $p = .0012$; Figure 4). Post hoc Welch's unequal variances *t* test demonstrated that both basal and apical ANFs from E15.5 ganglia could be strongly repelled by stripes containing 10, 20, or 40 μg/ml ephrin-A3-Fc (Figures 3(k,m) and 4), but E17.5 ANFs could only be strongly repelled by stripes containing 40 μg/ml ephrin-A3-Fc (Figures 3(l,n) and 4). As will be discussed, early sensitivity of ANFs to ephrinA3 could exclude them from the ventral CN, contributing to their initial termination in the dorsal CN.

3.4 | Reduced precision of tonotopic inputs from ANFs in the *Efna3*$^{-/-}$ mutant AVCN

We next asked whether ephrin-A3 is required in the CN to organize tonotopic precision of ANF inputs by using mice lacking the ephrin-A3 gene (*Efna3*$^{-/-}$ mice) to address our questions. Nylon filter paper

(a)

Three-Way ANOVA	α = 0.05						
Source of Variation	SS	DF	MS	F (DFn, DFd)	% of total variation	P value	Significant?
Ephrin-A3-Fc concentration (0-40 μg)	6.912	4	1.728	F (4, 85) = 45.28	59.11	<0.0001	Yes
(Basal vs Apical)	0.006634	1	0.006634	F (1, 85) = 0.1738	0.05673	0.6778	No
(E15.5 vs E17.5)	0.4288	1	0.4288	F (1, 85) = 11.24	3.667	0.0012	Yes
Interaction							
Ephrin-A3-Fc concentration x (Basal vs Apical)	0.2175	4	0.05437	F (4, 85) = 1.425	1.86	0.2327	No
Ephrin-A3-Fc concentration x (E15.5 vs E17.5)	0.6223	4	0.1556	F (4, 85) = 4.077	5.322	0.0045	Yes
(Basal vs Apical) x (E15.5 vs E17.5)	0.005811	1	0.005811	F (1, 85) = 0.1523	0.0497	0.6973	No
Ephrin-A3-Fc concentration x (Basal vs Apical) x (E15.5 vs E17.5)	0.2523	4	0.06308	F (4, 85) = 1.653	2.158	0.1685	No
Note: SS, sum of squares; df, degrees of freedom; MS, mean Square							

(b)

Welch's unequal variances t-test (two-tailed)				α = 0.05			
	E15.5_Basal				E17.5_Basal		
Ephrin-A3-Fc concentraion	neurites on labeled stripe / neurites on unlabled stripe (Mean±SD)	P value (vs 0 μg)	Significant?		neurites on labeled stripe / neurites on unlabled stripe (Mean±SD)	P value (vs 0 μg)	Significant?
0 μg	0.96 ± 0.07 (n = 4)				1.00 ± 0.01 (n = 3)		
2 μg	0.99 ± 0.07 (n = 6)	0.82	No		0.95 ± 0.12 (n = 6)	0.76	No
10 μg	0.52 ± 0.07 (n = 6)	0.0032	Yes		1.13 ± 0.08 (n = 5)	0.27	No
20 μg	0.50 ± 0.07 (n = 6)	0.0025	Yes		0.61 ± 0.14 (n = 4)	0.056	No
40 μg	0.31 ± 0.07 (n = 7)	0.0001	Yes		0.33 ± 0.05 (n = 6)	4.23×10^{-5}	Yes
	E15.5_Apical				E17.5_Apical		
Ephrin-A3-Fc concentraion	neurites on labeled stripe / neurites on unlabled stripe (Mean±SD)	P value (vs 0 μg)	Significant?		neurites on labeled stripe / neurites on unlabled stripe (Mean±SD)	P value (vs 0 μg)	Significant?
0 μg	0.96 ± 0.02 (n = 3)				1.08 ± 0.09 (n = 3)		
2 μg	0.98 ± 0.05 (n = 7)	0.75	No		1.03 ± 0.16 (n = 5)	0.84	No
10 μg	0.53 ± 0.08 (n = 4)	0.0075	Yes		0.73 ± 0.14 (n = 5)	0.12	No
20 μg	0.40 ± 0.07 (n = 5)	0.0011	Yes		0.66 ± 0.12 (n = 5)	0.049	Yes
40 μg	0.40 ± 0.02 (n = 8)	4.5×10^{-7}	Yes		0.37 ± 0.06 (n = 7)	0.0002	Yes

FIGURE 4 Quantification and statistics of the ephrin-A3 stripe assay. (a) A three-way ANOVA indicates that ephrin-A3 repels growing auditory nerve fibers (ANFs) in a dose-dependent manner. Basal and apical ANFs show no significant difference in their responses to ephrin-A3 repulsive effects. Instead, a significant change in sensitivity to ephrin-A3 repulsion is evident between ANFs from different developmental stages (E15.5 vs. E17.5). (b) Quantification and statistics of stripe assays of cochlear explants from distinct cochlear regions and different developmental stages [Color figure can be viewed at wileyonlinelibrary.com]

strips coated with NeuroVue red and maroon dyes were inserted into the mid-basal and apical turns of the cochlea in E18.5 heads. The dye was allowed to diffuse anterogradely through ANFs to the hindbrain. This enables us to trace innervation of distinct subsets of ANF inputs in the CN. For each tracing, the fraction of the AVCN area innervated by dye-labeled ANFs from the mid-basal or apical cochlear turn [(S_{mb}/S_{AVCN} × 100) or (S_a/S_{AVCN} × 100)] was normalized to the area of the NeuroVue-labeled spiral ganglion in the corresponding cochlear turn (sg_{mb} or sg_a) to obtain (S_{mb}/S_{AVCN} × 100)/sg_{mb} or (S_a/S_{AVCN} × 100)/sg_a.

In littermate controls, SGN afferents traced from the mid-basal or apical turn targeted to topographically distinct regions in the developing AVCN along the tonotopic axis (Figure 5(a)). The gross tonotopic targeting observed in the control was also preserved in the *Efna3*$^{-/-}$ mutant (Figure 5(b)). However, in the *Efna3*$^{-/-}$ mutant, the dye tracing from ANFs was more diffuse when compared to the control (Figure 5(a,b)). In control AVCN, clear segregation of the two dyes was observed (Figure 5(a)). In *Efna3*$^{-/-}$ AVCN, the areas targeted by ANFs labeled with the two dyes were adjacent to each other with very little segregation (Figure 5(b,d)). Welch's unequal variances *t* tests revealed that mid-basal ANFs innervated ~38% more area in *Efna3*$^{-/-}$ AVCN than in control AVCN ($p = .016$, $n = 5$), and apical ANFs targeted ~twice more area in *Efna3*$^{-/-}$ AVCN than in control AVCN ($p < .0001$, $n = 5$) (Figure 5(c)). Additionally, Welch's unequal variances *t* test also showed that the distance between S_{mb} and S_a was significantly decreased in *Efna3*$^{-/-}$ AVCN compared to control AVCN (Figure 5(d)). Thus, in *Efna3*$^{-/-}$ mutants, broad tonotopic segregation is maintained but precision of the tonotopic map is degraded at birth.

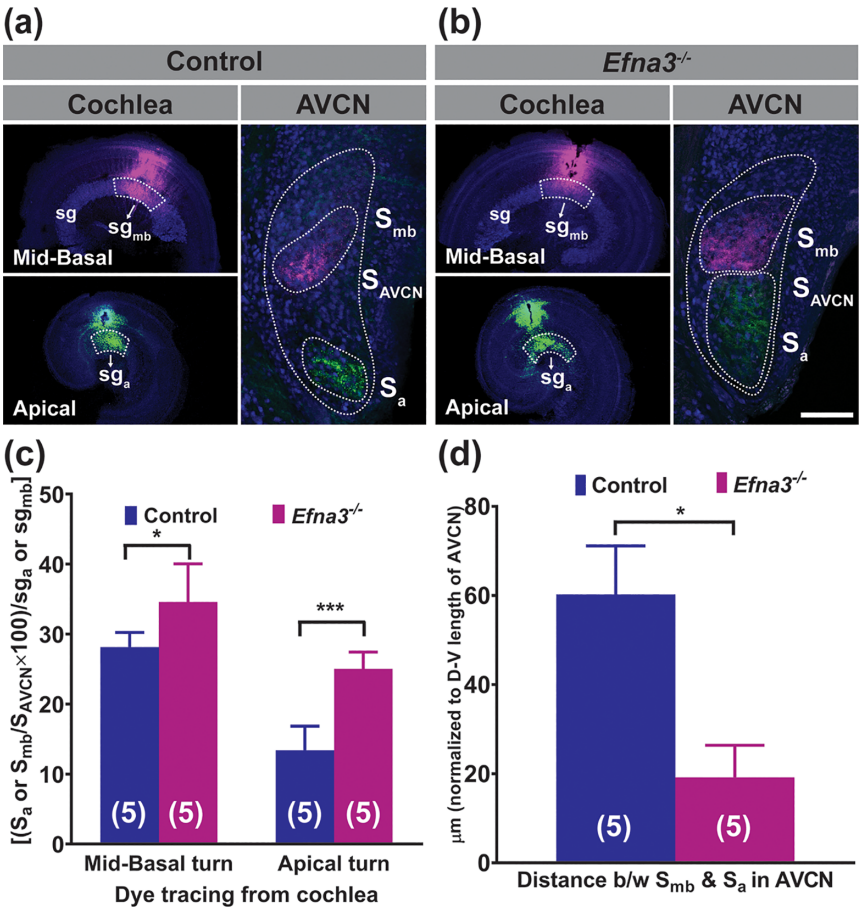

FIGURE 5 Reduced tonotopic precision of auditory nerve fiber (ANF) inputs in *Efna3*$^{-/-}$ mutant anteroventral cochlear nucleus (AVCN). (a,b) NeuroVue labeling of mid-basal (magenta) and apical cochlear turns (green), and their NeuroVue tracing in the AVCN (magenta: terminals from mid-basal ANFs; green: terminals from apical ANFs) in E18.5 control and *Efna3*$^{-/-}$ mice. The cochlea and AVCN were counterstained with anti-NeuN (blue) to reveal the cellular structure. The NeuroVue-labeled ANFs from mid-basal or apical cochlear turns target distinct regions along the tonotopic axis of the AVCN in both control and *Efna3*$^{-/-}$ mice. However, the dye tracing from *Efna3*$^{-/-}$ ANFs in the AVCN was more spread out when compared to the tracing from control ANFs. sg: spiral ganglion; sg_{mb} or sg_a: the area of the NeuroVue-labeled spiral ganglion in the mid-basal or apical cochlear turn; S_{mb} or S_a: the AVCN area innervated by NeuroVue-labeled ANFs from mid-basal or apical cochlear turns; S_{AVCN}: total AVCN area. Scale bar: 300 µm for cochleae and 100 µm for AVCN. (c) Welch's unequal variances *t* test shows that ANFs innervate a significantly larger area in *Efna3*$^{-/-}$ AVCN than in control AVCN. Mid-basal *Efna3*$^{-/-}$ ANFs target ~38% more area and apical *Efna3*$^{-/-}$ ANFs target about twice more area in the mutant AVCN when compared to the AVCN area targeted by control ANFs. Numbers on the bar indicate the sample size. Means ± *SD*s are shown. $^*p < .05$, $^{***}p < .001$. (d) Welch's unequal variances *t* test shows that the distance between S_{mb} and S_a is significantly less in *Efna3*$^{-/-}$ AVCN than in control AVCN. Numbers on the bar indicate the sample size. Means ± *SD*s are shown. $^*p < .05$ [Color figure can be viewed at wileyonlinelibrary.com]

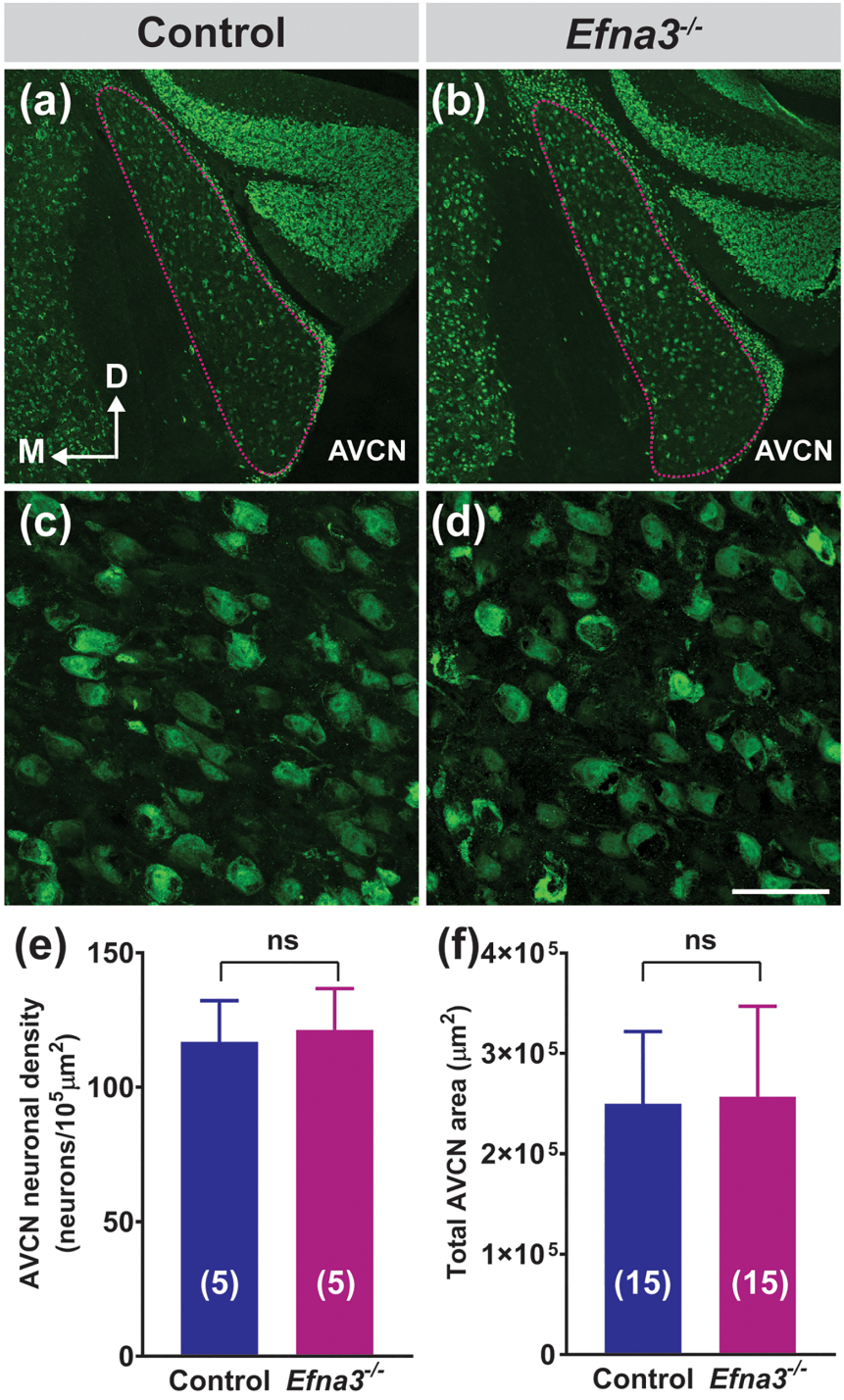

FIGURE 6 Anteroventral cochlear nucleus (AVCN) area and neuronal density in the AVCN are normal in *Efna3*$^{-/-}$ mutants. (a–d) Coronal brain sections through the AVCN from 6-week-old littermate control and an *Efna3*$^{-/-}$ mutant mice were stained for neuN. Magenta dotted lines outline the AVCN, as judged by neuN staining. The axis in (a) indicates the orientation of all the sections in the figure. D, dorsal; M, medial. Scale bar in (d), 150 µm for (a,b) and 50 µm for (c,d). (e–g) No significant difference of neuronal density in the AVCN and AVCN area between controls and *ephrin-A3*$^{-/-}$ mutants (Welch's *t* test) [Color figure can be viewed at wileyonlinelibrary.com]

(g)

Welch's t-test (α = 0.05, two-tailed)		
	AVCN neuronal density (neurons/10^5µm^2)	Total AVCN area (µm^2)
Control (Mean ± SD)	116.85 ± 15.34 (n=5)	263,031 ± 50,398 (n=15)
Efna3$^{-/-}$ (Mean ± SD)	121.31 ± 15.34 (n=5)	268,667 ± 79,401 (n=15)
P-value (control vs. a3$^{-/-}$)	0.66	0.82
Significant?	No	No

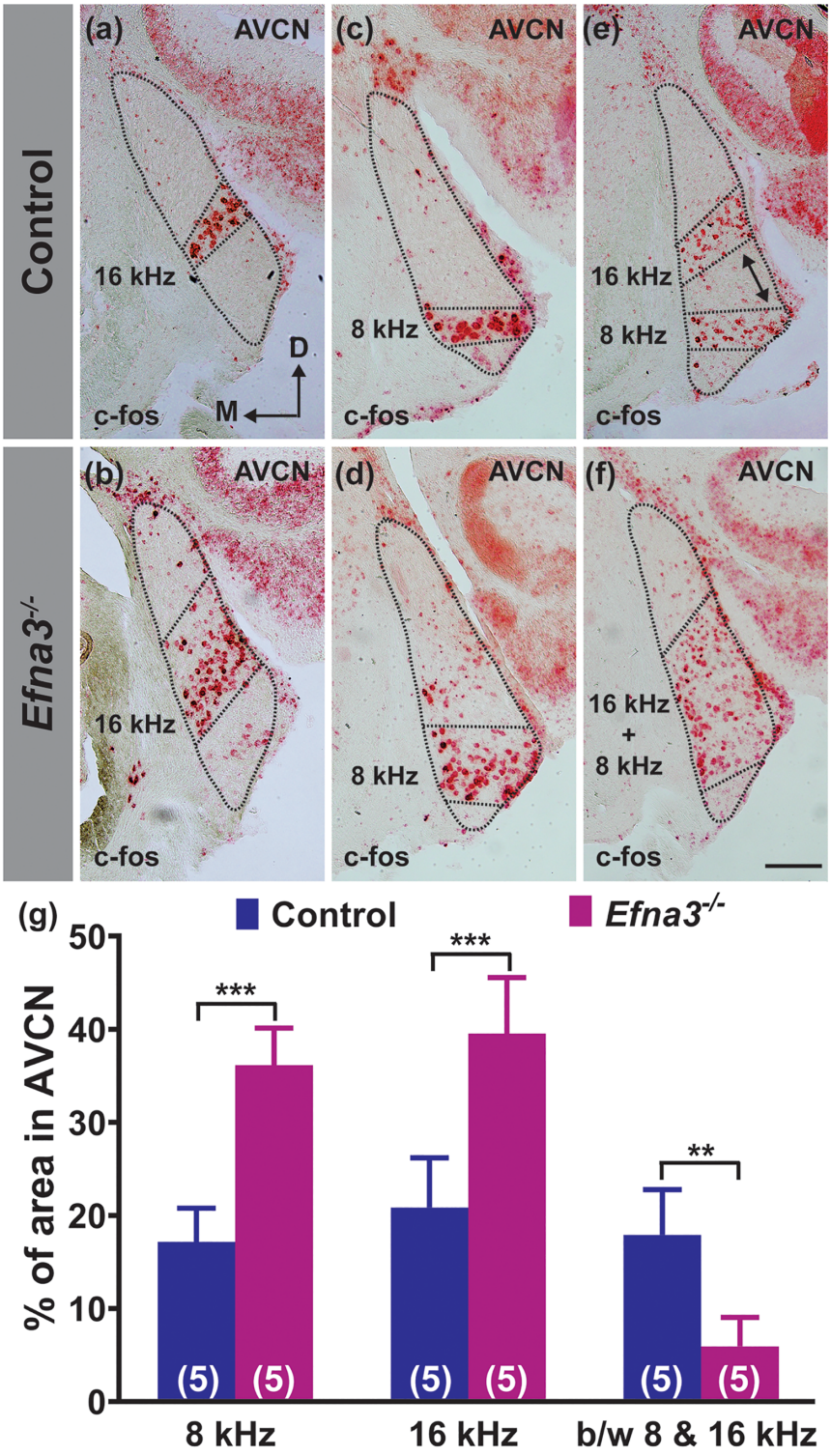

FIGURE 7 *c-fos* activation isofrequency bands are broadened in *Efna3*$^{-/-}$ mutant anteroventral cochlear nucleus (AVCN) upon pure tone stimulation. (a–f) *c-fos*-activated AVCN neurons detected by RNAScope in situ hybridization in response to stimulation of a single 16-kHz tone, a single 8-kHz tone, or simultaneous 16- and 8-kHz dual tones in control and *Efna3*$^{-/-}$ mutant AVCN. *c-fos*$^{+}$ bands in AVCN after 16-kHz stimulation or 8-kHz stimulation are broader in *Efna3*$^{-/-}$ mutants than in controls (a–d). Upon 16- and 8-kHz dual tone exposure, a separation zone between the two *c-fos*-activated bands can be readily detected in the controls, whereas no clear separation of *c-fos*$^{+}$ bands is observed in *Efna3*$^{-/-}$ mutants (e,f). Scale bar: 200 μm. (g) Quantification of *c-fos*-activated areas or separation areas between *c-fos*$^{+}$ bands normalized to total AVCN areas in response to stimulation of a 16-kHz tone, an 8-kHz tone, or simultaneous 16- and 8-kHz dual tones in control and *Efna3*$^{-/-}$ mutant AVCN. Numbers on the bar indicate the sample size. Means ± *SD*s are shown. $^{**}p < .01$, $^{***}p < .001$, Welch's unequal variances *t* test [Color figure can be viewed at wileyonlinelibrary.com]

3.5 | *Efna3*$^{-/-}$ AVCN show a broadening of neuronal c-fos activation upon pure tone exposure

In postnatal development, neuronal connectivity in the coarse tonotopic map undergoes axon refinement and synapse elimination due to spontaneous neuronal activity and post-hearing sensory experience to sharpen isofrequency bands and achieve high tonotopic resolution in the mature circuits (Clause et al., 2014; Jackson & Parks, 1982; Jhaveri & Morest, 1982; Leake et al., 2002). Degraded precision of tonotopic inputs from perinatal mutant ANFs raised the question of whether imprecise tonotopic connectivity may impair postnatal refinement and diminish tonotopic map resolution in adult *Efna3*$^{-/-}$ mutants. To test this possibility, we exposed awake, freely moving 5- to 7-week-old mice to 16-kHz tone pips, 8-kHz tone pips,

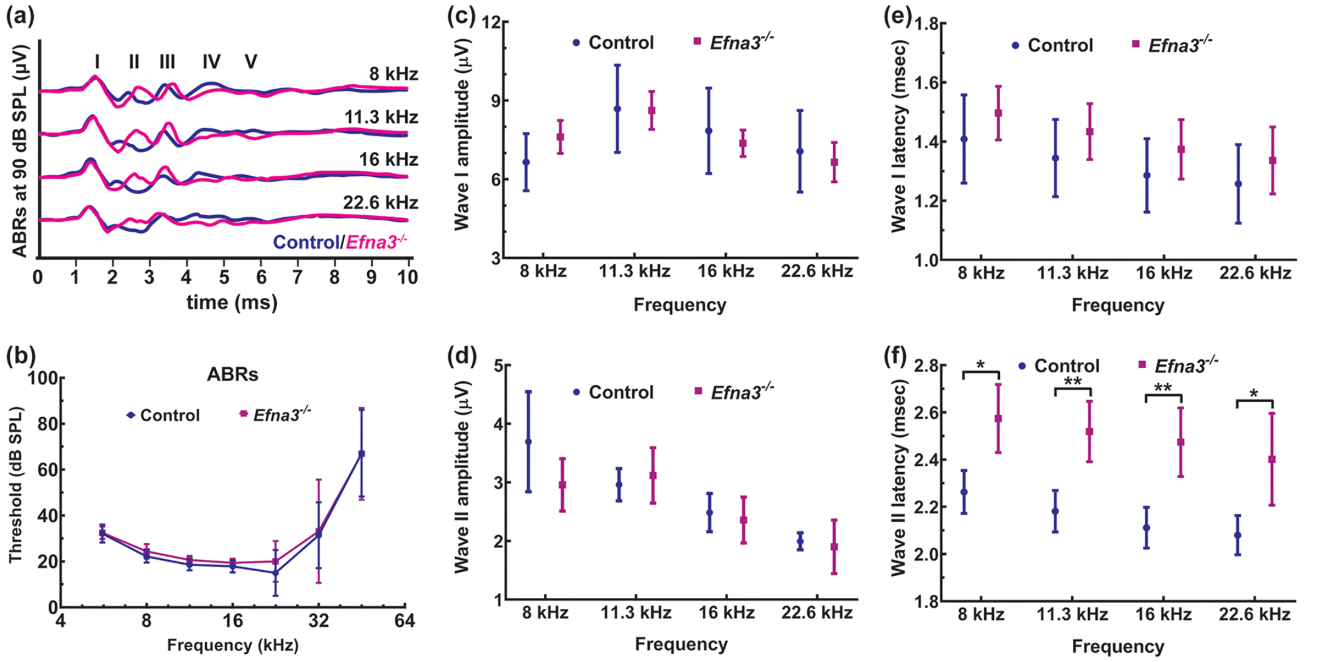

FIGURE 8 *Efna3*$^{-/-}$ mutants show normal hearing thresholds but a delayed Wave II in auditory brainstem responses (ABRs). (a) Representative ABR recordings from a 6-week-old littermate control (blue traces) and an *Efna3*$^{-/-}$ mutant (magenta traces) exposed to 8, 11.3, 16, or 22.6 kHz pure tone stimuli at intensity of 90 dB sound pressure level (SPL). Roman numerals mark the ABR waves. Wave I of ABRs are normal but Wave II are delayed in *Efna3*$^{-/-}$ mutants compared to control littermates. (b) Average ABR thresholds for seven littermate controls (blue) and eight *Efna3*$^{-/-}$ mutants (magenta) across frequency. No significant difference was observed between controls and *Efna3*$^{-/-}$ mutants (two-way ANOVA, $F_{(1,91)} = 0.6836$, $p = .4105$). (c,d) Average Wave I and Wave II amplitudes for seven littermate controls (blue) and eight *ephrin-A3*$^{-/-}$ mutants (magenta) in response to 8, 11.3, 16, or 22.6 kHz pure tone stimuli at intensity of 90 dB SPL. No significant difference of Wave I and II amplitudes was observed between controls and *Efna3*$^{-/-}$ mutants (two-way ANOVA; Wave I: $F_{(1,52)} = 4.222 \times 10^{-6}$, $p = .9984$; Wave II: $F_{(1,52)} = 0.3753$, $p = .5428$). (e,f) Average Wave I and II latencies for seven littermate controls (blue) and eight *Efna3*$^{-/-}$ mutants (magenta) in response to 8, 11.3, 16, or 22.6 kHz pure tone stimuli at intensity of 90 dB SPL. No significant difference of Wave I latencies was observed between controls and *Efna3*$^{-/-}$ mutants (two-way ANOVA, $F_{(1,52)} = 3.842$, $p = .0554$). However, Wave II of *Efna3*$^{-/-}$ mutants were significantly delayed when compared to controls (two-way ANOVA, $F_{(1,52)} = 44.23$, $p < .0001$; post hoc Welch's *t* test, $^{*}p < .05$, $^{**}p < .01$). Means ± *SD*s are shown in (b–f) [Color figure can be viewed at wileyonlinelibrary.com]

or simultaneous 16- and 8-kHz tone pips at 75 dB SPL for 90 min and evaluated induction of the immediate early gene *c-fos* by calculating the percentage of *c-fos*-positive area in the AVCN from the section containing the largest AVCN area. The total AVCN area and neuronal density in the AVCN were similar between controls and *Efna3*$^{-/-}$ mutants (Figure 6), suggesting that AVCN size and survival of AVCN neurons were not affected in *Efna3*$^{-/-}$ mutants. In controls, *c-fos*-positive isofrequency bands could be observed at different zones along the tonotopic axis in the AVCN upon pure tone exposure at 16 or 8 kHz (Figure 7(a,c)). In *Efna3*$^{-/-}$ mutant, pure tone stimulation also generated distinct *c-fos*-positive bands along the tonotopic axis in the AVCN but these *c-fos*-positive bands became broader in mutants than in controls (Figure 7(b,d)). Furthermore, stimulation of alternating 16- and 8-kHz tone pips induced two distinct segregated *c-fos*-positive bands in control AVCN but the same stimulation generated two overlapped isofrequency bands in a single large unresolved area in *Efna3*$^{-/-}$ AVCN (Figure 7(e,f)). Welch's *t* tests showed that 16- or 8-kHz stimulation generated approximately twice larger c-fos-positive area in *Efna3*$^{-/-}$ than in control AVCN ($p < .001$, $n = 5$ for each genotype in each group, for 16- or 8-kHz stimulation) and simultaneous 16- and 8-kHz stimulation resulted in a separation zone between two *c-fos*-positive bands around three times smaller in *Efna3*$^{-/-}$ than in control AVCN ($p = .002$, $n = 5$ for each genotype in each group) (Figure 7(g)). In summary, these results indicate that in the absence of ephrin-A3 molecules, auditory activation patterns are changed and the tonotopic specificity is degraded in the AVCN.

3.6 | *Efna3*$^{-/-}$ mutants have a normal hearing threshold but show a delayed ABR Wave II

Mice with defects in peripheral auditory circuits are known to have diminished auditory sensitivity, but mice with degraded tonotopic precision have been shown to have apparently normal hearing (Lu et al., 2014). To determine whether hearing is affected in *Efna3*$^{-/-}$ mutants with impaired tonotopy, we compared ABRs between 5- to 7-week-old control and *Efna3*$^{-/-}$ mutant mice in response to seven pure tone pips from 5.6 to 45.2 kHz. ABRs reflect the electrical responses of neurons in the cochlea and auditory brainstem to sound stimuli. The first wave of ABRs (Wave I) reflects the synchronous

firing of SGN axons and the second wave (Wave II) reflects the synchronous firing of globular cells near the eighth nerve root in the VCN (Melcher et al., 1996).

Both control and *Efna3*$^{-/-}$ mice produced characteristic ABR waveforms in response to all stimuli (Figure 8(a)). No significant difference was observed between controls and *Efna3*$^{-/-}$ mice in hearing thresholds, or the amplitude and latency of Wave I in response to 8–22.6 kHz tones at 90 dB SPL (Figure 8(b,c,e)) (two-way ANOVA, $n = 7$ controls and eight mutants; threshold: $F_{(1,91)} = 0.6836$, $p = .41$; amplitude: $F_{(1,52)} = 4.22 \times 10^{-6}$, $p = .9984$; latency: $F_{(1,52)} = 3.842$, $p = .0554$). This indicates that the function of the peripheral circuit in the cochlea is largely normal in *Efna3*$^{-/-}$ mice. In line with this, we did not observe obvious changes in wiring, gross cellular organization, olivocochlear efferent innervation, or neuronal cell density in adult *Efna3*$^{-/-}$ cochleae (Figure 9). However, the second wave of ABRs was delayed in *Efna3*$^{-/-}$ mutants in response to 8–22.6 kHz tones at 90 dB SPL (two-way ANOVA, $n = 7$ controls and eight mutants; threshold: $F_{(1,52)} = 44.23$, $p < .0001$), although its amplitude appears normal when compared to controls (two-way ANOVA, $n = 7$ controls and eight mutants; threshold: $F_{(1,52)} = 0.3753$, $p = .54$) (Figure 8(d,f)). The increased latency of the Wave II suggests that degraded tonotopic precision of ANF inputs may lead to delayed firing in some VCN neurons.

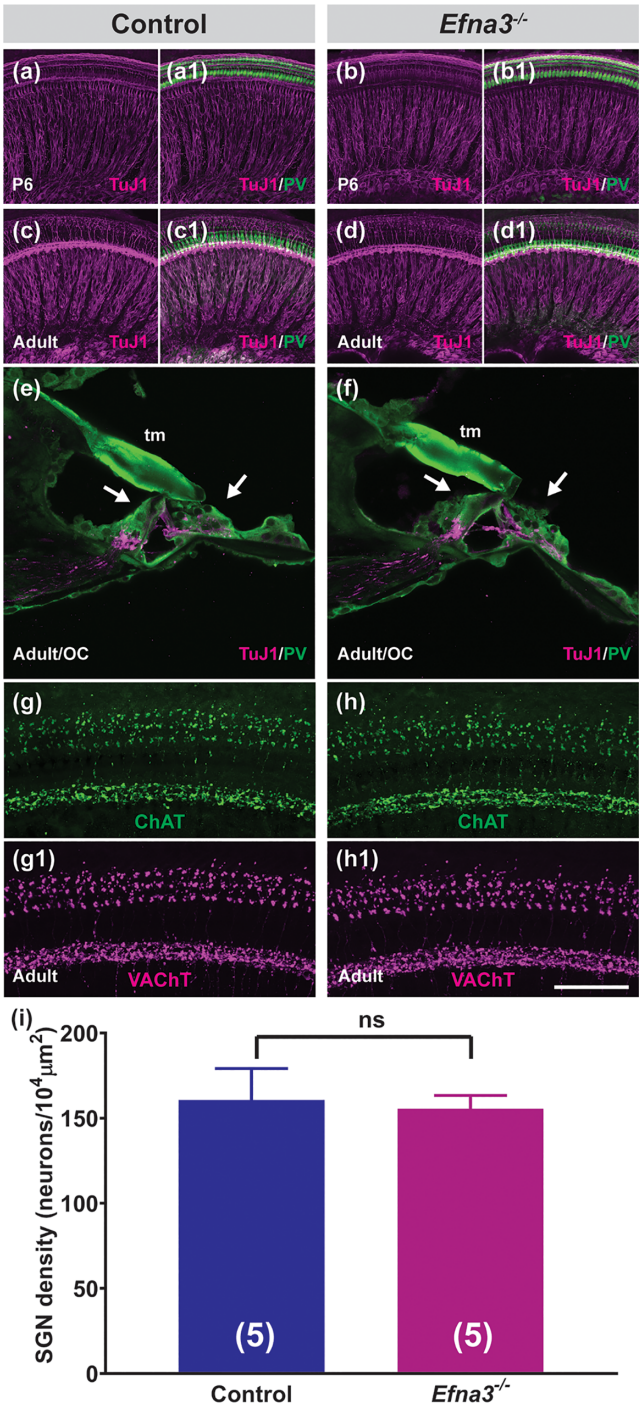

3.7 | *Efna3*$^{-/-}$ mutants exhibit impaired frequency discrimination

Although *Efna3*$^{-/-}$ mutants are still able to respond to sounds with normal sensitivity, they may have subtle deficits in processing sound information. In mutant mice with degraded tonotopic maps in the auditory brainstem, they exhibit deficits in frequency discrimination (Clause et al., 2014; Karmakar et al., 2017). To explore whether decreased tonotopic precision in *Efna3*$^{-/-}$ mutants could result in a similar functional defect, we used prepulse inhibition (PPI) of the ASR to assess sound frequency discrimination as described previously (Clause et al., 2011; Clause et al., 2017; Mwilambwe-Tshilobo et al., 2015). The ASR is a reflexive motor response to an unexpected loud sound that presents as a rapid contraction of skeletal muscles. In mice, ASR is measured by placing the animal on a platform that senses and transmits the downward force produced by the reflex. The ASR is attenuated when a weak prepulse sound is detected just before the

FIGURE 9 Basic wiring, gross cellular organization, olivocochlear efferent innervation, and spiral ganglion neuron (SGN) density are largely normal in *Efna3*$^{-/-}$ cochleae. (a–d1) Confocal stacks from P6 and 6-week-old control and *Efna3*$^{-/-}$ cochlear whole-mounts stained for parvalbumin to mark hair cells (green) and class III beta-tubulin (TuJ1) to label neuronal processes (magenta). Cochlear wiring is grossly normal in *Efna3*$^{-/-}$ mice. (e,f) Confocal stacks from transverse sections through 6-week-old control and *Efna3*$^{-/-}$ cochleae stained for parvalbumin to mark hair cells (green) and class III beta-tubulin (TuJ1) to label neuronal processes (magenta). Arrows indicate inner and outer hair cells. tm: tectorial membrane. Cellular organization of the organ of Corti (OC) and innervation of inner and outer hair cells are grossly normal in *Efna3*$^{-/-}$ mice. (g–h1) Projections of confocal stacks from 6-week-old control and *Efna3*$^{-/-}$ cochlear whole-mounts double stained for choline acetyltransferase (ChAT, green) and vesicular acetylcholine transporter (VAChT, magenta) to label the efferent innervation in cochleae. Olivocochlear efferent innervation is normal in *Efna3*$^{-/-}$ cochleae. Scale bar in (h1), 150 µm for (a–d1) and 50 µm for (e–h1). (i) No significant difference of SGN cell density between controls ($n = 5$) and *Efna3*$^{-/-}$ mice ($n = 5$) ($p = .60$, two-tailed Welch's t test) [Color figure can be viewed at wileyonlinelibrary.com]

startle-eliciting loud sound, a condition termed PPI. By providing a continuous background tone at a single frequency prior to the pulse and interrupting it with a different (prepulse) tone, the ability of the subject to distinguish the different tone from the background tone can be assessed: detection of the tone results in PPI, nondetection of the tone change results in no PPI (i.e., no reduction in force applied by the subject to the platform compared to no prepulse). We used a background tone of 16 kHz and seven prepulse tones ranging from 15.92 to 12 kHz.

No significant difference of body weight was found between 5- to 7-week-old controls and *Efna3*$^{-/-}$ mutants (19.55 ± 1.35 g in eight controls vs. 19.29 ± 2.66 g in six mutants, $p = .81$, Welch's t test), suggesting *Efna3*$^{-/-}$ mutants should generate a downward force comparable to controls if their ASR is normal. Both control and *Efna3*$^{-/-}$ mice showed a similar ASR in response to the startle stimulus. The average ASR amplitude was not significantly different between the two groups (2.00 ± 0.22 arbitrary units [AU] in eight controls vs. 2.10 ± 0.25 AU in six mutants, $p = .47$, Welch's t test)

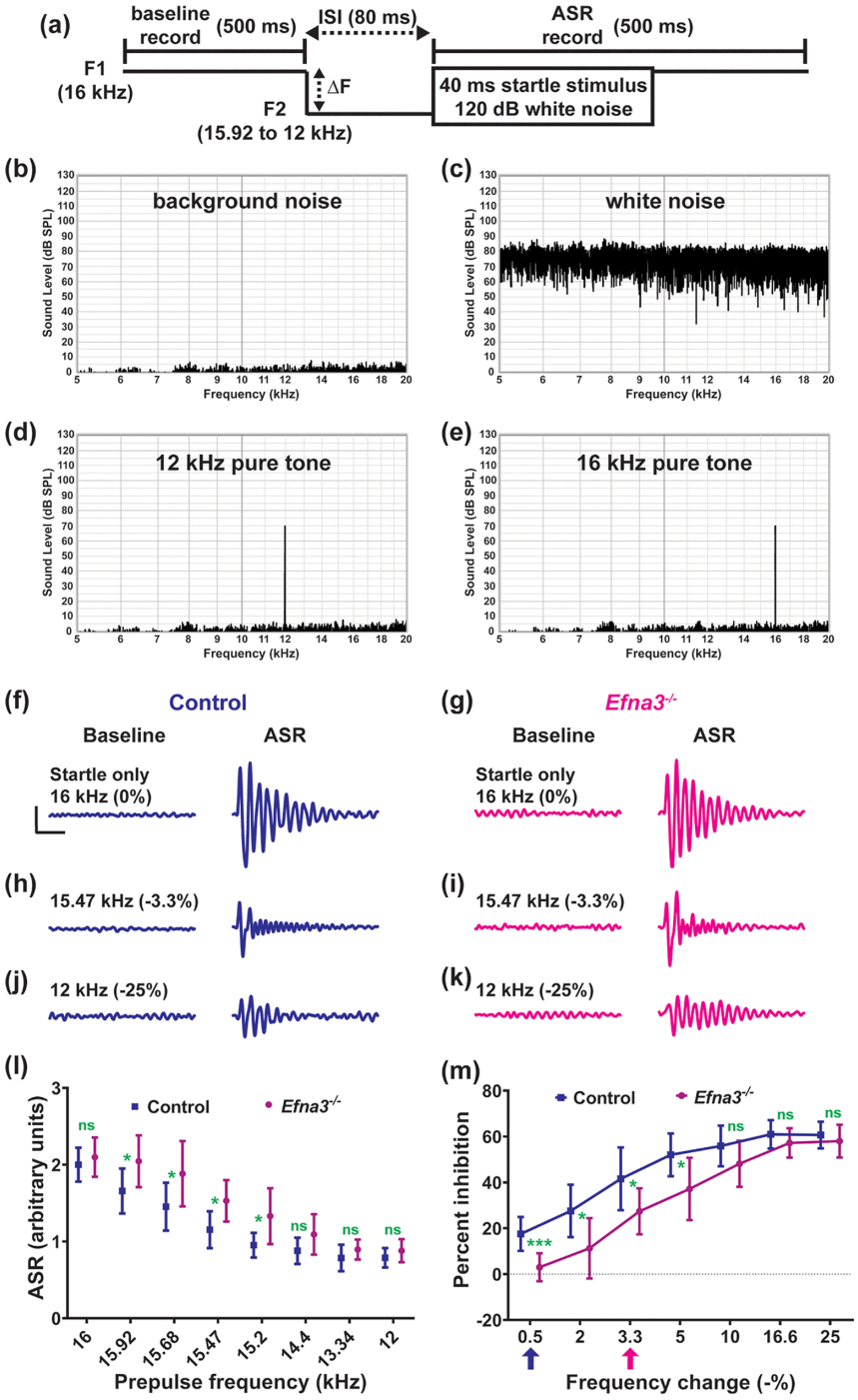

FIGURE 10 Legend on next page.

TABLE 2 Two-way ANOVA of ASR and PPI between controls and *Efna3*$^{-/-}$ mutants in frequency discrimination assay

Two-way ANOVA of ASR amplitudes	$\alpha = .05$						
Source of variation	**SS**	**df**	**MS**	***F* (dfn, dfd)**	**% of total variation**	***p*-Value**	**Significant?**
Different prepulse frequencies	21.17	7	3.024	$F_{(7,96)} = 47.67$	71.1	**<.0001**	**Yes**
Control vs. *Efna3*$^{-/-}$	1.861	1	1.861	$F_{(1,96)} = 29.33$	6.251	**<.0001**	**Yes**
Interaction (prepulse frequencies × control vs. *A3*$^{-/-}$)	0.5172	7	0.07389	$F_{(7,96)} = 1.165$	1.737	.3304	No
Two-way ANOVA of PPI	$\alpha = .05$						
Source of variation	**SS**	**df**	**MS**	***F* (dfn, dfd)**	**% of total variation**	***p*-Value**	**Significant?**
Frequency change −%	30,742	6	5124	$F_{(6,84)} = 55.86$	74.33	**<.0001**	**Yes**
Control vs. *Efna3*$^{-/-}$	2686	1	2686	$F_{(1,84)} = 29.29$	6.496	**<.0001**	**Yes**
Interaction (frequency change −% × control vs. a*3*$^{-/-}$)	674.5	6	112.4	$F_{(6,84)} = 1.225$	1.631	.3015	No

Bold values are significance.
Abbreviations: ASR, acoustic startle response; df, degrees of freedom; MS, mean square; PPI, prepulse inhibition; SS, sum of squares.

TABLE 3 Quantification and statistics of ASR in frequency discrimination assays

Welch's unequal variances *t* test			$\alpha = .05$	
Prepulse frequency (kHz)	**Control ASR (mean ± *SD*, *n* = 8)**	***Efna3*$^{-/-}$ ASR (mean ± *SD*, *n* = 6)**	***p*-Value (con vs. a*3*$^{-/-}$)**	**Significant?**
16	2.00 ± 0.22	2.10 ± 0.26	.47	No
15.92	1.66 ± 0.29	2.05 ± 0.34	**.024**	**Yes**
15.68	1.45 ± 0.31	1.88 ± 0.43	**.033**	**Yes**
15.47	1.15 ± 0.24	1.53 ± 0.27	**.011**	**Yes**
15.2	0.95 ± 0.16	1.33 ± 0.36	**.028**	**Yes**
14.4	0.88 ± 0.17	1.09 ± 0.26	.06	No
13.34	0.79 ± 0.17	0.89 ± 0.13	.1	No
12	0.79 ± 0.13	0.88 ± 0.15	.12	No

Bold values are significance.
Abbreviation: ASR, acoustic startle response.

(Figure 10(f,g), and Tables 2–4 for statistical analyses), indicating that the function of startle reflex circuitry is normal in *Efna3*$^{-/-}$ mice. Both control and *Efna3*$^{-/-}$ mutants showed an inhibition of the ASR when the startle stimulus is preceded by a frequency shift from the background frequency. The inhibition increased when the magnitude of the frequency change increased and plateaued around 60% inhibition for a

FIGURE 10 *Efna3*$^{-/-}$ mutants show impaired prepulse inhibition (PPI) of the acoustic startle response (ASR) for detecting changes in sound frequencies. (a) Trial schematic for the ASR-based frequency discrimination assay. ISI: interstimulus interval; F1: background frequency; F2: prepulse frequency; Δ*F*: frequency change. (b) Background noise in the anechoic chamber. (c) White noise at 120 dB sound pressure level (SPL) for the startle stimulus. (d,e) Prepulse frequencies are seven tones from 15.92 to 12 kHz at 70 dB SPL. Only the 12 kHz prepulse tone is shown. The background frequency is 16 kHz tone at 70 dB SPL. (f–k) Representative recording traces of baseline activity and ASRs from a control (blue) and an *Efna3*$^{-/-}$ mutant (magenta). Baseline or ASR traces represent the force measured during the first or the second 500-ms recording period. Scale bar in (f), 1.0 arbitrary unit of force, 100 ms. Both control and *Efna3*$^{-/-}$ mice show a normal ASR in response to the startle stimulus. A change from the 16 kHz background tone to prepulse tones (15.47 kHz, −3.3% change or 12 kHz, −25% change) before the startle stimulus inhibited the ASR in both control and *Efna3*$^{-/-}$ mice. However, the amount of inhibition elicited by the small 3.3% negative frequency change was less in *Efna3*$^{-/-}$ mutants when compared to control. The large 25% frequency change elicits similar inhibition between control and *Efna3*$^{-/-}$ mice. (l) Average ASR amplitudes for eight controls (blue) and six *Efna3*$^{-/-}$ mutants (magenta) for each trial type. Means ± *SD*s are shown. No significant difference of ASR amplitudes was observed between controls and *Efna3*$^{-/-}$ mutants in response to the startle-only stimulus ($p = .47$, Welch's *t* test). The ASR magnitude elicits by small negative frequency changes (0.5–5%) was significant smaller in controls than in *Efna3*$^{-/-}$ mutants (ns: no significance, *$p < .05$, two-way ANOVA with post hoc Welch's *t* test). (m) Average percent inhibition of the ASR elicited by prepulse frequency changes at various magnitudes for eight controls (blue) and six *Efna3*$^{-/-}$ mutants (magenta). Means ± *SD*s are shown. *Efna3*$^{-/-}$ mutants show significantly reduced PPI for small negative frequency changes (0.5–5%), indicating an impaired ability to detect small frequency changes. Arrows indicate discrimination threshold, the smallest frequency change that elicited a significant inhibition of the ASR ($p < .05$, one-tailed Welch's *t* test compared to zero frequency change). *Efna3*$^{-/-}$ mutants have an elevated discrimination threshold [Color figure can be viewed at wileyonlinelibrary.com]

TABLE 4 Quantification and statistics of PPI in frequency discrimination assays

Welch's unequal variances *t* test			$\alpha = .05$	
Frequency change (−%)	Control % inhibition (mean ± *SD*, $n = 8$)	*Efna3*$^{-/-}$ % inhibition (mean ± *SD*, $n = 6$)	*p*-Value (con vs. a3$^{-/-}$)	Significant?
0.5	17.52% ± 7.39%	3.01% ± 6.10%	**.00085**	**Yes**
2	27.57% ± 11.45%	11.25% ± 13.15%	**.0178**	**Yes**
3.3	41.56% ± 13.67%	27.39% ± 10.04%	**.0226**	**Yes**
5	52.02% ± 9.33%	37.15% ± 13.56%	**.0249**	**Yes**
10	55.88% ± 8.86%	48.14% ± 10.04%	.0822	No
16.6	60.98% ± 6.19%	57.20% ± 6.38%	.1447	No
25	60.65% ± 5.82%	57.99% ± 7.13%	.2366	No

Bold values are significance.
Abbreviation: PPI, prepulse inhibition.

TABLE 5 One-tailed Welch's *t* test was used to compared PPI elicited by no frequency change and PPI elicited by negative frequency changes from 16-kHz background tone to determine frequency discrimination threshold

Welch's unequal variances *t* test (one-tailed)		$\alpha = .05$		
Frequency change (−%) to elicit PPI	Control ($n = 8$) *p*-Value (no frequency change ASR vs. −% frequency change ASR)	Inhibition significant?	*Efna3*$^{-/-}$ ($n = 6$) *p*-Value (no frequency change ASR vs. −% frequency change ASR)	Inhibition significant?
0.5	**0.01008**	**Yes (discrimination threshold)**	0.37752	No
2	0.00061	Yes	0.15083	No
3.3	1.83×10^{-6}	Yes	**0.00103**	**Yes (discrimination threshold)**
5	3.22×10^{-9}	Yes	0.00103	Yes
10	1.23×10^{-9}	Yes	2.13×10^{-5}	Yes
16.6	1.03×10^{-9}	Yes	2.14×10^{-7}	Yes
25	9.83×10^{-12}	Yes	7.71×10^{-8}	Yes

Bold values are significance.
Abbreviation: PPI, prepulse inhibition.

frequency shift around 16.6% (Figure 10(m) and Table 4). However, PPI elicited by small negative frequency changes (0.5–5%) was significantly reduced in *Efna3*$^{-/-}$ mutants compared to controls (two-way ANOVA, $F_{(1,84)} = 29.29$, $p < .0001$; post hoc Welch's *t* test, $p < .05$ for all frequency changes between 0.5 and 5%) (Figure 10(h,i,l,m), and Table 2). Additionally, the frequency discrimination threshold (defined as the smallest frequency change that elicited a significant inhibition of the ASR when compared to inhibition elicited by no frequency change using one-tailed Welch's *t* test) was elevated in *Efna3*$^{-/-}$ mutants compared to controls (Figure 10(m) and Table 5). The smallest frequency change, 0.5%, could already elicit a significant inhibition in controls ($p = .01$). By comparison, the ASR of *Efna3*$^{-/-}$ mutants was not significantly inhibited until the frequency change of the prepulse tone reached 3.3% (0.5–2% [$p > .15$], 3.3% [$p = .001$]). As PPI elicited by large frequency changes (10–25%) was still similar between controls and *Efna3*$^{-/-}$ mutants (Figure 10(j–m) and Table 4), it is unlikely that reduced PPI elicited by small frequency changes in mutants is caused by a deficit in circuitry that mediates PPI. Therefore, the ability of *Efna3*$^{-/-}$ mice to detect sound frequency changes was impaired, consistent with the observation of an altered *c-fos* activation pattern.

4 | DISCUSSION

Here, we demonstrate that ephrin-A3 molecules show differential expression along the tonotopic axis in the developing CN, and their absence disrupts tonotopic mapping, acoustic processing, and sound discrimination. Together, our findings suggest a model for how ephrin-A3 might influence tonotopic map formation in the CN (Figure 11). Ephrin-A3 molecules are differentially expressed along the tonotopic axis in the CN during the emergence of the tonotopic map (Figure 11(a)). Correspondingly, ANFs innervate CN in a developmental gradient during these stages. Future high-frequency ANFs from early-born basal SGNs start to invade the CN from the ventral side around 2–3 days earlier than future low-frequency ANFs from the late-born apical SGNs. Ephrin-Eph signaling only occurs at sites of close cell–cell interaction to mediate axon targeting at choice points. When early-arriving basal ANFs navigate into the ventral part of the CN, a higher concentration of ephrin-A3 prevents axon terminals stabilizing on neurons in this region, similar to the mechanism used in retinocollicular mapping of the visual system (Feldheim et al., 2000), so these future high-frequency ANFs continue growing toward the

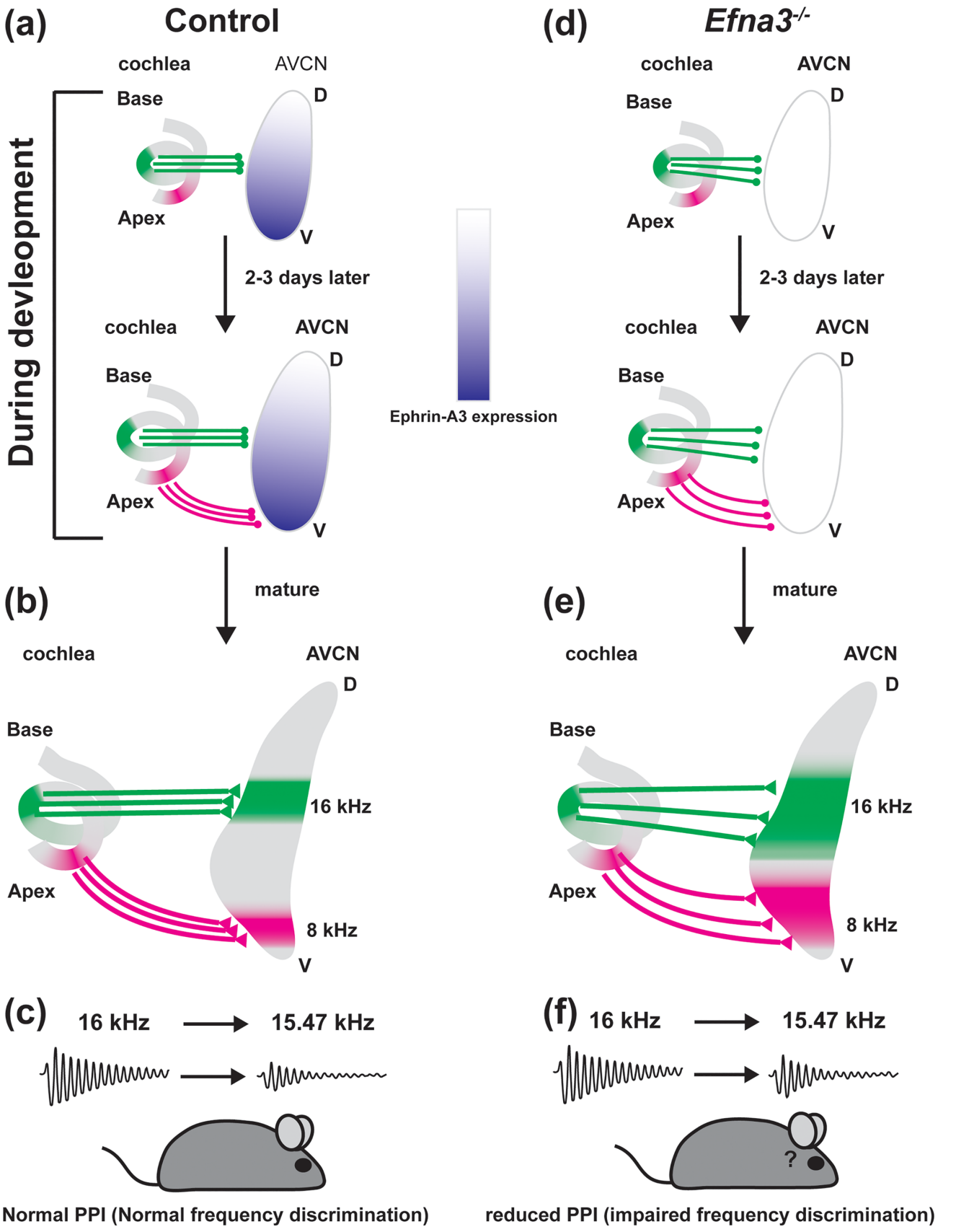

FIGURE 11 Legend on next page.

dorsal end. After 2–3 days, future low-frequency ANFs arrive in the ventral CN and are no longer strongly sensitive to ephrin-A3 due to a developmental reduction in the response to ephrin-A3, allowing them to maintain their terminals on neurons in this territory and innervate the ventral region (Figure 11(a,b)). In the absence of ephrin-A3, high-frequency ANFs may start to terminate more ventrally in the CN or fail to withdraw what would normally be transient branches (Figure 11(d)), causing a degraded tonotopic map and impaired sound discrimination in mutant animals (Figure 11(e,f)). While our data are consistent with this model, we cannot exclude the possibility that knocking out ephrin-A3 disrupts central projections primarily by disrupting some other less direct parsimonious mechanism in the peripheral circuit or in the CN.

In *Efna3*$^{-/-}$ mutants, the gross tonotopic segregation is still maintained, indicating that in addition to ephrin-A3 molecules, other guidance molecules are also involved in regulating tonotopic mapping in the CN. Indeed, in the visual system, in order to orchestrate the formation of precise topographic maps of the retinocollicular projections, multiple ephrin and Eph molecules are expressed in complementary gradients in the retina and superior colliculus (Triplett & Feldheim, 2012). A similar mechanism could be employed by the auditory system to establish tonotopic maps. Other ephrins or Eph molecules could be differentially expressed along the tonotopic axis in an opposite pattern complementary to ephrin-A3 molecules to restrict future low-frequency ANFs to target to the dorsal region of the developing CN. Concordantly with this, in addition to ephrin-A3, several ephrins and Ephs show high expression in the developing rhombomeres between E15.5 and E18.5, including ephrinB2/B3, EphA4/A5/A8/A10, and EphB1/B2 (Allen Mouse Brain Atlas). EphrinB2 and EphA4 are also demonstrated to be necessary for accurate auditory activation patterns in the CN and several ephrin/Eph mutant mice exhibit altered ABRs (Defourny, 2019; Miko et al., 2007; Miko et al., 2008). Furthermore, diffusible axon guidance molecules are also needed to serve as long-range cues to guide future high-frequency or low-frequency ANFs to grow toward the dorsal end or stay in the ventral side of the CN. How these ephrins and Eph receptors influence tonotopic map formation, which Eph receptors mediate ephrin-A3 effects, and whether other families of axon guidance molecules also participate in the process will require additional studies.

We observed a developmentally reduced sensitivity to ephrin-A3 in ANFs. One possibility that could account for the decreased response to ephrin-A3 is a decreased level of EphA receptors at the cell surface by endocytosis of EphA receptors, which has been observed during development of the retinocollicular topographic map (Yoo et al., 2011). Other mechanisms that could account for the reduced response to ephrin-A3 are a negative regulation of Eph receptors by protein tyrosine phosphatases (Shintani et al., 2006) or a downregulation/negative regulation of intracellular signaling effectors (Schmucker & Zipursky, 2001). Whether EphA4 and EphA7 receptors are involved in mediating responses of ANFs to ephrin-A3 and how the receptor signaling is regulated to modulate ephrin-A3 effects are currently under investigation.

Homeodomain (Hox) transcription factors are known to be one of the key regulators of Eph receptor expression. In mice lacking *Hoxa2* and *Hoxb2* genes in AVCN neurons, mutant mice presented defects that were similar to those observed in *Efna3*$^{-/-}$ mutants (Karmakar et al., 2017). *Hox2* mutants also exhibit a degraded tonotopic map, an altered auditory *c-fos* activation pattern, and impaired sound frequency discrimination. In addition to Hox transcription factors, classical morphogens, such as Wnt proteins, have been shown to regulate the expression of ephrins/Ephs in mediating intestinal epithelial cell positioning or medial-lateral retinocollicular topographic mapping (Batlle et al., 2002; Schmitt et al., 2006). These observations suggest that anterior–posterior positional cues from distinct Hox genes may orchestrate the nonuniformly distributed morphogens to establish the differential expression pattern of ephrins/Ephs in proper locations during tonotopic mapping in the auditory brainstem.

Finally, comparing the roles of ephrin/Eph signaling in auditory circuit development in a variety of model systems will deepen our understanding of why particular ephrins and Ephs are deployed in different regions of the nervous system and help us understand their roles in human development. Developmental perturbations in the central auditory pathway frequently result in central auditory processing disorders, a heterogeneous group of conditions estimated to affect 2–3% of children with no known cause (Chermak et al., 1997). Identifying the molecular cues that underlie establishment of tonotopy may help us elucidate the pathogenesis of these disorders.

ACKNOWLEDGMENTS

This work was supported by the National Institutes of Health (R15DC016407 to M. W. R. and R15DC017866 to W. Y.). The authors thank Mr Joseph Schluep (Loyola University Chicago) for help

FIGURE 11 Proposed model for ephrin-A3's role in CN tonotopic mapping and sound discrimination. (a) During embryonic development, ephrin-A3 molecules are differentially expressed along the tonotopic axis in the CN. Neurogenesis of spiral ganglion neurons (SGNs) occurs in a basal to apical progression along the cochlea. Auditory nerve fibers (ANFs) of the early-born SGNs from basal/middle regions of the cochlea innervate the CN 2–3 days earlier than ANFs of the late-born apical SGNs. A higher concentration of ephrin-A3 in the ventral region of the CN prevents these early-arriving ANFs from stabilizing their terminals in the ventral territory and innervate areas more dorsally. After 2–3 days, the response of ANFs to ephrin-A3 decreases, allowing late-arriving apical ANFs to target to the ventral portion of the CN. (b,c) When the auditory system matures, the cochlea and CN establish a normal tonotopic arrangement of neuronal connectivity where basal ANFs project to the dorsal part of the CN and apical ANFs target to the ventral side of the CN, forming precise isofrequency bands to allow animals to discriminate sounds even with subtle frequency changes. (d–f) In *Efna3*$^{-/-}$ mutants, early-arriving ANFs from the base or middle region of the cochlea may start to terminate in areas more ventrally in the CN due to a lack of ephrin-A3 in the ventral region, leading to a degraded tonotopic map and impaired ability to detect sound frequency changes when the animal matures [Color figure can be viewed at wileyonlinelibrary.com]

with making the cylinder animal enclosure for pure tone exposure. The authors also thank Dr Lisa Goodrich (Harvard Medical School) for her critical reading of the manuscript.

CONFLICT OF INTEREST

The authors declare no conflict of interests.

AUTHOR CONTRIBUTIONS

Natalia Hoshino, **Vincent C.-F. Chen**, **M. William Rochlin**, and **Wei-Ming Yu**: Conceived of and designed the study. **Natalia Hoshino**, **Yazan Altarshan**, **Ahmad Alzein**, **Amali M. Fernando**, **M. William Rochlin**, and **Wei-Ming Yu**: Performed the experiments and collect the data. **Natalia Hoshino**, **Yazan Altarshan**, **Hieu T. Nguyen**, **Emma F. Majewski**, and **Wei-Ming Yu**: Analyzed the data and conducted statistical analysis. **Wei-Ming Yu**: Wrote the manuscript.

PEER REVIEW

The peer review history for this article is available at https://publons.com/publon/10.1002/cne.25213.

DATA AVAILABILITY STATEMENT

The data that support the findings of this study are available from the corresponding author upon reasonable request.

ORCID

Ahmad Alzein https://orcid.org/0000-0002-5369-9033

Wei-Ming Yu https://orcid.org/0000-0002-8408-2888

REFERENCES

Batlle, E., Henderson, J. T., Beghtel, H., van den Born, M. M., Sancho, E., Huls, G., Meeldijk, J., Robertson, J., van de Wetering, M., Pawson, T., & Clevers, H. (2002). Beta-catenin and TCF mediate cell positioning in the intestinal epithelium by controlling the expression of EphB/ephrinB. *Cell*, *111*(2), 251–263. https://doi.org/10.1016/s0092-8674(02)01015-2

Carmona, M. A., Murai, K. K., Wang, L., Roberts, A. J., & Pasquale, E. B. (2009). Glial ephrin-A3 regulates hippocampal dendritic spine morphology and glutamate transport. *Proceedings of the National Academy of Sciences of the United States of America*, *106*(30), 12524–12529. https://doi.org/10.1073/pnas.0903328106

Chermak, G. D., Musiek, F. E., & Craig, C. H. (1997). *Central auditory processing disorders: New perspectives*. Singular Pub Group.

Clause, A., Kim, G., Sonntag, M., Weisz, C. J., Vetter, D. E., Rűbsamen, R., & Kandler, K. (2014). The precise temporal pattern of prehearing spontaneous activity is necessary for tonotopic map refinement. *Neuron*, *82*(4), 822–835. https://doi.org/10.1016/j.neuron.2014.04.001

Clause, A., Lauer, A. M., & Kandler, K. (2017). Mice lacking the Alpha9 subunit of the nicotinic acetylcholine receptor exhibit deficits in frequency difference limens and sound localization. *Frontiers in Cellular Neuroscience*, *11*, 167. https://doi.org/10.3389/fncel.2017.00167

Clause, A., Nguyen, T., & Kandler, K. (2011). An acoustic startle-based method of assessing frequency discrimination in mice. *Journal of Neuroscience Methods*, *200*(1), 63–67. https://doi.org/10.1016/j.jneumeth.2011.05.027

Coate, T. M., Raft, S., Zhao, X., Ryan, A. K., Crenshaw, E. B., & Kelley, M. W. (2012). Otic mesenchyme cells regulate spiral ganglion axon fasciculation through a Pou3f4/EphA4 signaling pathway. *Neuron*, *73*(1), 49–63. https://doi.org/10.1016/j.neuron.2011.10.029

Cramer, K. S., & Gabriele, M. L. (2014). Axon guidance in the auditory system: Multiple functions of Eph receptors. *Neuroscience*, *277*, 152–162. https://doi.org/10.1016/j.neuroscience.2014.06.068

Cramer, K. S., & Miko, I. J. (2016). Eph-ephrin signaling in nervous system development. *F1000Res*, *5*, 413. https://doi.org/10.12688/f1000research.7417.1

Defourny, J. (2019). Eph/ephrin signalling in the development and function of the mammalian cochlea. *Developmental Biology*, *449*(1), 35–40. https://doi.org/10.1016/j.ydbio.2019.02.004

Egea, J., & Klein, R. (2007). Bidirectional Eph-ephrin signaling during axon guidance. *Trends in Cell Biology*, *17*(5), 230–238. https://doi.org/10.1016/j.tcb.2007.03.004

Farago, A. F., Awatramani, R. B., & Dymecki, S. M. (2006). Assembly of the brainstem cochlear nuclear complex is revealed by intersectional and subtractive genetic fate maps. *Neuron*, *50*(2), 205–218. https://doi.org/10.1016/j.neuron.2006.03.014

Fekete, D. M., Rouiller, E. M., Liberman, M. C., & Ryugo, D. K. (1984). The central projections of intracellularly labeled auditory nerve fibers in cats. *The Journal of Comparative Neurology*, *229*(3), 432–450. https://doi.org/10.1002/cne.902290311

Feldheim, D. A., Kim, Y. I., Bergemann, A. D., Frisén, J., Barbacid, M., & Flanagan, J. G. (2000). Genetic analysis of ephrin-A2 and ephrin-A5 shows their requirement in multiple aspects of retinocollicular mapping. *Neuron*, *25*(3), 563–574. https://doi.org/10.1016/s0896-6273(00)81060-0

Fujiyama, T., Yamada, M., Terao, M., Terashima, T., Hioki, H., Inoue, Y. U., Inoue, T., Masuyama, N., Obata, K., Yanagawa, Y., Kawaguchi, Y., Nabeshima, Y. I., & Hoshino, M. (2009). Inhibitory and excitatory subtypes of cochlear nucleus neurons are defined by distinct bHLH transcription factors, Ptf1a and Atoh1. *Development*, *136*(12), 2049–2058. https://doi.org/10.1242/dev.033480

Huffman, K. J., & Cramer, K. S. (2007). EphA4 misexpression alters tonotopic projections in the auditory brainstem. *Developmental Neurobiology*, *67*(12), 1655–1668. https://doi.org/10.1002/dneu.20535

Jackson, H., & Parks, T. N. (1982). Functional synapse elimination in the developing avian cochlear nucleus with simultaneous reduction in cochlear nerve axon branching. *The Journal of Neuroscience*, *2*(12), 1736–1743.

Jhaveri, S., & Morest, D. K. (1982). Sequential alterations of neuronal architecture in nucleus magnocellularis of the developing chicken: A Golgi study. *Neuroscience*, *7*(4), 837–853. https://doi.org/10.1016/0306-4522(82)90046-x

Kandler, K., Clause, A., & Noh, J. (2009). Tonotopic reorganization of developing auditory brainstem circuits. *Nature Neuroscience*, *12*(6), 711–717.

Kania, A., & Klein, R. (2016). Mechanisms of ephrin-Eph signalling in development, physiology and disease. *Nature Reviews. Molecular Cell Biology*, *17*(4), 240–256. https://doi.org/10.1038/nrm.2015.16

Karmakar, K., Narita, Y., Fadok, J., Ducret, S., Loche, A., Kitazawa, T., Genoud, C., di Meglio, T., Thierry, R., Bacelo, J., Lüthi, A., & Rijli, F. M. (2017). Hox2 genes are required for tonotopic map precision and sound discrimination in the mouse auditory brainstem. *Cell Reports*, *18*(1), 185–197. https://doi.org/10.1016/j.celrep.2016.12.021

Kim, Y. J., Ibrahim, L. A., Wang, S. Z., Yuan, W., Evgrafov, O. V., Knowles, J. A., Wang, K., Tao, H. W., & Zhang, L. I. (2016). EphA7 regulates spiral ganglion innervation of cochlear hair cells. *Developmental Neurobiology*, *76*(4), 452–469. https://doi.org/10.1002/dneu.22326

Knöll, B., Weinl, C., Nordheim, A., & Bonhoeffer, F. (2007). Stripe assay to examine axonal guidance and cell migration. *Nature Protocols*, *2*(5), 1216–1224. https://doi.org/10.1038/nprot.2007.157

Koundakjian, E. J., Appler, J. L., & Goodrich, L. V. (2007). Auditory neurons make stereotyped wiring decisions before maturation of their targets.

The Journal of Neuroscience, *27*(51), 14078–14088. https://doi.org/10.1523/JNEUROSCI.3765-07.2007

Leake, P. A., Snyder, R. L., & Hradek, G. T. (2002). Postnatal refinement of auditory nerve projections to the cochlear nucleus in cats. *The Journal of Comparative Neurology*, *448*(1), 6–27. https://doi.org/10.1002/cne.10176

Lu, C. C., Cao, X. J., Wright, S., Ma, L., Oertel, D., & Goodrich, L. V. (2014). Mutation of Npr2 leads to blurred tonotopic organization of central auditory circuits in mice. *PLoS Genetics*, *10*(12), e1004823. https://doi.org/10.1371/journal.pgen.1004823

Macova, I., Pysanenko, K., Chumak, T., Dvorakova, M., Bohuslavova, R., Syka, J., Fritzsch, B., & Pavlinkova, G. (2019). Neurod1 is essential for the primary tonotopic organization and related auditory information processing in the midbrain. *The Journal of Neuroscience*, *39*(6), 984–1004. https://doi.org/10.1523/JNEUROSCI.2557-18.2018

Martin, M. R., & Rickets, C. (1981). Histogenesis of the cochlear nucleus of the mouse. *The Journal of Comparative Neurology*, *197*(1), 169–184. https://doi.org/10.1002/cne.901970113

Matei, V., Pauley, S., Kaing, S., Rowitch, D., Beisel, K. W., Morris, K., Feng, F., Jones, K., Lee, J., & Fritzsch, B. (2005). Smaller inner ear sensory epithelia in Neurog 1 null mice are related to earlier hair cell cycle exit. *Developmental Dynamics*, *234*(3), 633–650. https://doi.org/10.1002/dvdy.20551

Melcher, J. R., Guinan, J. J., Knudson, I. M., & Kiang, N. Y. (1996). Generators of the brainstem auditory evoked potential in cat. II. Correlating lesion sites with waveform changes. *Hearing Research*, *93*(1–2), 28–51. https://doi.org/10.1016/0378-5955(95)00179-4

Miko, I. J., Henkemeyer, M., & Cramer, K. S. (2008). Auditory brainstem responses are impaired in EphA4 and ephrin-B2 deficient mice. *Hearing Research*, *235*(1–2), 39–46. https://doi.org/10.1016/j.heares.2007.09.003

Miko, I. J., Nakamura, P. A., Henkemeyer, M., & Cramer, K. S. (2007). Auditory brainstem neural activation patterns are altered in EphA4- and ephrin-B2-deficient mice. *The Journal of Comparative Neurology*, *505*(6), 669–681. https://doi.org/10.1002/cne.21530

Muniak, M. A., Rivas, A., Montey, K. L., May, B. J., Francis, H. W., & Ryugo, D. K. (2013). 3D model of frequency representation in the cochlear nucleus of the CBA/J mouse. *The Journal of Comparative Neurology*, *521*(7), 1510–1532. https://doi.org/10.1002/cne.23238

Mwilambwe-Tshilobo, L., Davis, A. J., Aizenberg, M., & Geffen, M. N. (2015). Selective impairment in frequency discrimination in a mouse model of tinnitus. *PLoS One*, *10*(9), e0137749. https://doi.org/10.1371/journal.pone.0137749

Pierce, E. T. (1967). Histogenesis of the dorsal and ventral cochlear nuclei in the mouse. An autoradiographic study. *The Journal of Comparative Neurology*, *131*(1), 27–54. https://doi.org/10.1002/cne.901310104

Ruben, R. J. (1967). Development of the inner ear of the mouse: A radioautographic study of terminal mitoses. *Acta Otolaryngol*, *220*, 221–244.

Saul, S. M., Brzezinski, J. A., Altschuler, R. A., Shore, S. E., Rudolph, D. D., Kabara, L. L., … Glaser, T. (2008). Math5 expression and function in the central auditory system. *Molecular and Cellular Neurosciences*, *37*(1), 153–169. https://doi.org/10.1016/j.mcn.2007.09.006

Scheffel, J. L., Mohammed, S. S., Borcean, C. K., Parng, A. J., Yoon, H. J., Gutierrez, D. A., & Yu, W.-M. (2020). Spatiotemporal analysis of cochlear nucleus innervation by spiral ganglion neurons that serve distinct regions of the cochlea. *Neuroscience*, *446*, 43–58.

Schmitt, A. M., Shi, J., Wolf, A. M., Lu, C. C., King, L. A., & Zou, Y. (2006). Wnt-Ryk signalling mediates medial-lateral retinotectal topographic mapping. *Nature*, *439*(7072), 31–37. https://doi.org/10.1038/nature04334

Schmucker, D., & Zipursky, S. L. (2001). Signaling downstream of Eph receptors and ephrin ligands. *Cell*, *105*(6), 701–704. https://doi.org/10.1016/s0092-8674(01)00391-9

Shepard, A. R., Scheffel, J. L., & Yu, W. M. (2019). Relationships between neuronal birthdates and tonotopic positions in the mouse cochlear nucleus. *The Journal of Comparative Neurology*, *527*(5), 999–1011. https://doi.org/10.1002/cne.24575

Shintani, T., Ihara, M., Sakuta, H., Takahashi, H., Watakabe, I., & Noda, M. (2006). Eph receptors are negatively controlled by protein tyrosine phosphatase receptor type O. *Nature Neuroscience*, *9*(6), 761–769. https://doi.org/10.1038/nn1697

Siddiqui, S. A., & Cramer, K. S. (2005). Differential expression of Eph receptors and ephrins in the cochlear ganglion and eighth cranial nerve of the chick embryo. *The Journal of Comparative Neurology*, *482*(4), 309–319. https://doi.org/10.1002/cne.20396

Treffy, R. W., Collins, D., Hoshino, N., Ton, S., Katsevman, G. A., Oleksiak, M., Runge, E. M., Cho, D., Russo, M., Spec, A., Gomulka, J., Henkemeyer, M., & Rochlin, M. W. (2016). Ephrin-B/EphB signaling is required for normal innervation of lingual gustatory papillae. *Developmental Neuroscience*, *38*(2), 124–138. https://doi.org/10.1159/000444748

Triplett, J. W., & Feldheim, D. A. (2012). Eph and ephrin signaling in the formation of topographic maps. *Seminars in Cell & Developmental Biology*, *23*(1), 7–15. https://doi.org/10.1016/j.semcdb.2011.10.026

Yang, T., Kersigo, J., Wu, S., Fritzsch, B., & Bassuk, A. G. (2017). Prickle1 regulates neurite outgrowth of apical spiral ganglion neurons but not hair cell polarity in the murine cochlea. *PLoS One*, *12*(8), e0183773. https://doi.org/10.1371/journal.pone.0183773

Yoo, S., Kim, Y., Noh, H., Lee, H., Park, E., & Park, S. (2011). Endocytosis of EphA receptors is essential for the proper development of the retinocollicular topographic map. *The EMBO Journal*, *30*(8), 1593–1607. https://doi.org/10.1038/emboj.2011.44

Yu, W. M., Appler, J. M., Kim, Y. H., Nishitani, A. M., Holt, J. R., & Goodrich, L. V. (2013). A Gata3-Mafb transcriptional network directs post-synaptic differentiation in synapses specialized for hearing. *eLife*, *2*, e01341. https://doi.org/10.7554/eLife.01341

How to cite this article: Hoshino, N., Altarshan, Y., Alzein, A., Fernando, A. M., Nguyen, H. T., Majewski, E. F., Chen, V. C.-F., Rochlin, M. W., & Yu, W.-M. (2021). Ephrin-A3 is required for tonotopic map precision and auditory functions in the mouse auditory brainstem. *Journal of Comparative Neurology*, *529*(16), 3633–3654. https://doi.org/10.1002/cne.25213